ADDIS ABABA UNIVERSITY

COLLEGE OF TECHNOLOGY AND BUILT ENVIRONMENT

SCHOOL OF CHEMICAL AND BIO ENGINEERING

Removal of an Emerging Pharmaceutical Pollutant (Ibuprofen) from Aqueous Solution Using Magnetized Spent Coffee Ground Biochar - Chitosan Composite: Optimization, Isotherms, and Adsorption Kinetics

A Master of Science Thesis Submitted to the School of Chemical and Bio Engineering in Partial Fulfilment of the Requirements for the Degree of Master of Science in Chemical Engineering (Environmental Engineering)

By

Solomon Chekole Birhanu

Advisor: Dr. Shimelis Kebede Kassahun

OCTOBER 2025

ADDIS ABABA, ETHIOPIA

STATEMENT OF THE AUTHOR

I undersigned author hereby declare and affirm that this thesis, titled "**Removal of an Emerging Pharmaceutical Pollutant (Ibuprofen) from Aqueous Solution using Magnetized Spent Coffee Ground Biochar-Chitosan Composite: Optimization, Isotherms, and Adsorption Kinetics**," is the result of my own research and efforts toward my MSc degree. It has not been submitted, in whole or in part, for any other academic degree or professional qualification. I have acknowledged all sources of information through appropriate references.

Solomon Chekole Birhanu	_____	_____
Student's Name	Signature	Date

APPROVAL SHEET

This is to certify that the thesis prepared by Mr. Solomon Chekole, entitled "**Removal of an Emerging Pharmaceutical Pollutant (Ibuprofen) from Aqueous Solution using Magnetized Spent Coffee Ground Biochar-Chitosan Composite: Optimization, Isotherms, and Adsorption Kinetics**," has been submitted as partial fulfillment of the requirements for the degree of Master of Science in Chemical Engineering (Environmental Engineering Stream). It complies with the university regulations and meets the accepted standards for content, quality, and originality.

Approved by the Examination Committee

Dr. Zinnabu Tassew Internal Examiner	_____ Signature	_____ Date
Dr. Brook Tesfamichael External Examiner	_____ Signature	_____ Date
Dr. Shimelis Kebede Advisor	_____ Signature	_____ Date
Dr. Shimelis Kebede Chair Person	_____ Signature	_____ Date

ACKNOWLEDGEMENTS

First and foremost, I would like to express my gratitude to Almighty God for guiding me throughout this journey. I extend a special thanks to my advisor, Dr. Shimelis Kebede, whose exceptional guidance and dedication exceeded all expectations. His support was instrumental not only in the success of this work but also in my academic and personal development. I am also grateful to ISID-Ethiopia for their financial and consultative support, which made this journey possible. Additionally, I appreciate all my teachers, laboratory technicians, and the staff at the School of Chemical and Bioengineering for their unwavering commitment to the growth of their students. Lastly, I would like to thank my family and friends for their support.

ABSTRACT

Pharmaceutical pollutants, such as ibuprofen, are persistent environmental contaminants that threaten both flora and fauna. This study focused on synthesizing and characterizing a magnetized composite of spent coffee grounds biochar and chitosan for removing ibuprofen from synthetic wastewater. The composite adsorbent was developed using a co-precipitation method, varying the ratios of spent coffee grounds biochar to chitosan at 27:75, 50:50, and 75:25. Surface functional groups, morphology, specific surface area, elemental composition, and crystal structure were analyzed using Fourier Transform Infrared Spectroscopy (FTIR), Scanning Electron Microscopy (SEM), Brunauer-Emmett-Teller (BET) analysis, Energy Dispersive X-ray Spectroscopy (EDX), and X-ray Diffraction (XRD). Operational parameters for adsorption included initial ibuprofen concentration, pH, contact time, and adsorbent dosage. A statistical experimental design, specifically the Response Surface Methodology Central Composite Design, explored the interactions among these parameters to identify optimal conditions for ibuprofen removal. Analysis of Variance (ANOVA) was used for statistical evaluation. The BET, FTIR, SEM, XRD, and EDX analyses demonstrated that the magnetized composite had a high surface area of 524.65 m^2/g, essential functional groups (C–H, C=O, N–H, Fe–O) for ibuprofen binding, a porous and agglomerated morphology, dominant magnetite crystalline peaks alongside an amorphous organic matrix, and an elemental composition rich in Fe, O, and C, confirming successful integration into a uniform composite structure. The maximum ibuprofen removal efficiency achieved was 96.7% under optimal conditions: a pH of 4.5, an adsorbent dosage of 2.0 g/L, an initial ibuprofen concentration of 5 mg/L, and a contact time of 80 minutes. All selected parameters significantly influenced the performance of the synthesized composite adsorbent. The reusability of the composite under optimal conditions showed minimal variation in removal efficiency after five cycles of adsorption-desorption experiments were conducted. In conclusion, the composite adsorbent exhibited notable properties, enabling it to successfully remove ibuprofen from wastewater, making it an appropriate technique for environmental remediation.

Keywords: Spent Coffee Ground Biochar, Ibuprofen, Adsorption, Optimization, Kinetic Study.

TABLE OF CONTENTS

STATEMENT OF THE AUTHOR ..... **ii**

APPROVAL SHEET ..... **iii**

ACKNOWLEDGEMENTS ..... **iv**

ABSTRACT ..... **v**

LIST OF TABLES ..... **x**

LIST OF FIGURES ..... **xi**

LIST OF TABLES IN THE APPENDIX ..... **xii**

LIST OF ABBREVIATIONS AND ACRONYMS ..... **xiii**

CHAPTER ONE **1**

INTRODUCTION **1**

1.1. Background 1

1.2. Problem Statement 2

1.3. Research objectives 4

1.3.1. General objective 4

1.3.2. Specific Objectives 4

1.4. Significance of the Study 4

1.5. Scope of the Study 4

CHAPTER TWO **6**

LITERATURE REVIEW **6**

2.1. Water Pollution 6

2.2. Pharmaceuticals 7

2.3. Sources and pathways of pharmaceutical pollutants into the aquatic environment 8

2.4. Classifications of Pharmaceuticals 8

2.4.1. Analgesics and anti-inflammatories 9

2.4.2. Antibiotics 10

2.4.3. Antidepressants 11

2.5. Ibuprofen (IBP) 11
2.5.1. Sources and Occurrence of Ibuprofen (IBP) 12
2.5.2. Health Impacts and Toxicity of Ibuprofen (IBP) 14
2.6. Ibuprofen (IBP) Removal Methods from Aqueous Solutions 15
2.7. Adsorption 16
2.7.1. Physical Adsorption 16
2.7.2. Chemical Adsorption 16
2.8. Factors Affecting Adsorption Process 17
2.8.1. Initial Ibuprofen Concentration 17
2.8.2. pH 17
2.8.3. Contact Time 17
2.8.4. Adsorbent Dosage 18
2.9. Spent Coffee Ground (SCG) 18
2.9.1. Spent Coffee Ground Biochar (SCGB) 19
2.10. Chitosan 19
2.11. Polyvinyl Alcohol (PVA) 20
2.12. Magnetite 21
2.13. Summary of Previous Studies on the Removal of IBP 21
CHAPTER THREE 23
MATERIALS AND METHODS 23
3.1. Chemicals and Equipment 23
3.1.1. Chemicals and Reagents 23
3.1.2. Apparatus and Equipment 23
3.2. Raw Material Treatment and Sample Preparation 24
3.2.1. Raw Material Collection 24
3.3. Spent Coffee Ground (SCG) Characterization 24
3.3.1. Proximate Analysis of Spent Coffee Ground (SCG) 24

3.4. Synthesis of Spent Coffee Ground Biochar (SCGB) 25
3.5. Preparation of Magnetite (Fe_3O_4) 26
3.6. Preparation of Magnetized SCGB-Chitosan Composite 26
3.7. Physicochemical characterization of magnetized SCGB-Chitosan composite 27
3.7.1. Specific surface area characterization 27
3.7.2. XRD analysis 28
3.7.3. FTIR Analysis 28
3.7.4. SEM Analysis 28
3.8. Preparation of adsorbate solution 29
3.9. Adsorption Experiment 30
3.10. Study of Interaction Effect of Process Parameters and Model Evaluation Using Central-Composite Design Response Surface Method 31
3.11. Independent Factors and their Coded Levels for CCD Experiments 31
3.12. Optimization of Process Parameters and Statistical Analysis 33
3.13. Adsorption Isotherms and Kinetic Studies 33
3.13.1. Adsorption Isotherms 33
3.13.2. Kinetic Studies 34
3.14. Reusability Test 36
CHAPTER FOUR 37
RESULTS AND DISCUSSION 37
4.1. Yield of Spent Coffee Ground Biochar (SCGB) 37
4.2. Characterization of SCGBs and SCGB-Magnetite-Chitosan-PVA Composites 37
4.2.1. Proximate analysis of SCG 37
4.2.2. Surface area analysis of biochars, magnetite, and composites 38
4.2.3. FTIR analysis of biochars and composites 38
4.2.4. XRD analysis 40
4.2.5. Scanning Electron Microscope (SEM) Analysis 41

4.2.6. Energy Dispersive X-ray Spectroscopy (EDX) Analysis 42
4.3. Experimental Runs Based on Central Composite Design (CCD) 43
4.4.1. Sequential Model Sum of Squares 45
4.4.2. Analysis of Variance (ANOVA) 45
4.4.3. Fit Statistics 47
4.4.4. Diagnostic Plots 47
4.4.5. Combined Effects of the Independent Variables 49
4.5. Statistical optimization of process variables 53
4.6. Adsorption Isotherm and Kinetic Studies 53
4.6.1. Adsorption Isotherms 53
4.6.2. Adsorption Kinetic Study 55
4.7. Reusability 57
CHAPTER FIVE 59
CONCLUSIONS AND RECOMMENDATIONS 59
5.1. Conclusions 59
5.2. Recommendations 59
REFERENCES 61
APPENDICES 71

LIST OF TABLES

Table 2.1: Major Pharmaceutical pollutants 9
Table 2.2: Chemical and physical properties of IBU 12
Table 3.1: Preparation and sample codes for the biochars and composites 27
Table 3.2: Absorbance value of IBP concentration at 222 nm 29
Table 3.3: Independent factors and their coded level for CCD experiment 31
Table 3.4: CCD design matrix for four factors 32
Table 4.1: Production yield of Biochar for various Temperatures 37
Table 4.2: Proximate Analysis of SCG 37
Table 4.3: BET surface area of Biochars, magnetite, and composites 38
Table 4.4: CCD Experimental runs with factor levels and response data 44
Table 4.5: Sequential model sum of squares 45
Table 4.6: ANOVA for the quadratic model fitted to the experimental data 46
Table 4.7: Fit summary for the developed model 47
Table 4.8: Optimization constraints on operational factors and response. 53
Table 4.9: Isotherm model parameters for IBP adsorption onto Magnetized SCGB-Chitosan composite 54
Table 4.10: Pseudo first order, pseudo second order, and IPD kinetic models' parameters. 56

LIST OF FIGURES

Figure 2.1: Cumulative API concentrations across different countries.....7
Figure 2.2: The structure of IBU.....11
Figure 2.3: Sources and occurrence of IBP.....13
Figure 2.4: Pathway of IBP entering into food web.....14
Figure 2.5: Structure of Chitosan.....20
Figure 2.6: Structure of PVA.....20
Figure 3.1: Process flow diagram of the experimental work.....24
Figure 3.2: Calibration curve for IBP.....30
Figure 4.1: FTIR spectra of (a) Biochars and (b) Composites.....40
Figure 4.2: XRD pattern of composite (75:25).....41
Figure 4.3: SEM images of Composite (75:25) at resolutions of (a) 500, (b) 1k, (c) 3k, and (d) 10k.....42
Figure 4.4: EDX elemental analysis of composite (75:25).....43
Figure 4.5: Normal plot of Residuals for IBP removal efficiency.....48
Figure 4.6: Actual vs predicted values for IBP removal efficiency.....49
Figure 4.7: Interaction effect of (a) pH Vs initial concentration of IBP, (b) pH Vs adsorbent dosage, (c) pH Vs time, (d) Initial concentration Vs adsorbent dosage, (e) Initial concentration Vs time, and (f) adsorbent dosage Vs time.....**Error! Bookmark not defined.**
Figure 4.8: Adsorption Isotherm models of (a) Langmuir and (b) Freundlich.....55
Figure 4.9: Reaction kinetics models of (a) PFO, (b) PSO and (c) IPD.....57
Figure 4.10: The reusability of the composite adsorbent (75:25).....58
Figure C.1: Photograph confirmations for Experimental procedures.....74

LIST OF TABLES IN THE APPENDIX

Table A.1: Build information for the model 71
Table A.2: Model summary statistics 71
Table B.1: Coefficients in terms of coded factors 72
Table B.2: Actual and coded model equations..... 73

LIST OF ABBREVIATIONS AND ACRONYMS

API	Active Pharmaceutical Ingredients
ASTM	American Society for Testing Materials
BET	Brunauer-Emmett-Teller
CBD	Central Business District
DNA	Deoxyribonucleic Acid
EIA	Environmental Impact Assessment
FTIR	Fourier Transform Infrared Spectroscopy
IBP	Ibuprofen
IPD	Intraparticle Diffusion
IUPAC	International Union of Pure and Applied Chemistry
JCPDS	Joint Committee on Powder Diffraction Standards
LCA	Life Cycle Assessment
NSAID	Non-Steroidal anti-inflammatory Drugs
PFO	Pseudo-First-Order
PPCP	Pharmaceutical and Personal Care Products
PSO	Pseudo-Second-Order
PVA	Polyvinyl Alcohol
RSM	Response Surface Methodology
SCG	Spent Coffee Ground
SCGB	Spent Coffee Ground Biochar
SEM	Scanning Electron Microscope
UNESCO	United Nations Educational, Scientific, and Cultural Organization

UV-vis	Ultraviolet visible Spectroscopy
WHO	World Health Organization
WWTP	Waste Water Treatment Plant
XRD	X-ray Diffraction Spectroscopy

CHAPTER ONE

INTRODUCTION

1.1. Background

One of the topical issues of our age is environmental pollution. Industrialization, agriculture, natural factors, and poor water supply and sewage system facilities are some of the factors that have led to serious degradation of the environment, especially the pollution of the water (Lin et al., 2022; Xing et al., 2023). Water, an important component of life on earth, is very susceptible to pollution, making water pollution a major health concern of the people, particularly in developing nations such as Ethiopia (Kassahun et al., 2025).

There is a wide range of pollutants including persistent inorganic substances such as heavy metals and organic compounds like pharmaceuticals, pesticides, endocrine disruptors, and personal care products which represent a significant global concern. These pollutants negatively impact on the life of plants and animals in addition to human health (Vasilachi et al., 2021). Over the last several decades, the pharmaceutical sphere of production and consumption has begun to increase due to the development of medical science (Gkika et al., 2023). Now some 3000 compounds are used as pharmaceuticals, and quantities of production have reached hundreds of tons every year. Anti-inflammatory drugs, antibiotics, and analgesics are the most widely used medications in the world (Ortúzar et al., 2022).

Drugs are commonly found in the discharge of Wastewater Treatment Plants (WWTPs) all over the world. This pollution is because when humans and animals ingest these substances they are not fully absorbed by the body and therefore they find their way to the environment. The unceasing availability of the pharmaceuticals in the ecosystem mostly relates to their non-biodegradability and is partially treated in WWTPs (J. F. Shaheen et al., 2024).

Non-Steroidal Anti-inflammatory Drugs (NSAIDs) are widely prescribed type of drugs, the main purpose of which is to relieve fever, pain, rheumatoid arthritis, and osteoarthritis (Samal et al., 2022). One of the most common is Ibuprofen (IBP) which has been the most investigated due to its commonness in aquatic ecosystems and is one of the most commonly manufactured pharmaceuticals (J. F. Shaheen et al., 2024). IBP is usually found in wastewater since this medication is common and not taken out in treatment (Davarnejad et al., 2018). It has been reported in research that NSAIDs have concentrations of 1.1 to 55 mg/L in Africa with

particular reports of 221 mg/L in South Africa and 1.4 mg/L in Turkey. The levels of surface water contamination in Africa have been recorded to be 0.68 to 85 mg/L, Brazil 20 mg/L and China 5.4 mg/L. Also, the presence of IBP in tap water has become a topic of great concern, with traces being found ranging between 11-39 ng/L in Spain, 24-47 ng/L in Iran, 2.5-56 ng/L in France, 16 ng/L in Japan, and 8 ng/L in Sweden (Rashid Ahmed et al., 2024). IBP may have a negative effect on aquatic environment through interfering with the growth and reproductive functions of aquatic organisms and through modifying the necessary microbial communities that support ecosystem health. On additional basis, the build-up of IBP in drinking water is potentially dangerous to human health because it is associated with negative impacts on the liver, kidney, and the gastrointestinal system (Xing et al., 2023). At a concentration of as low as 1 μg/L, IBP may affect the processes of reproduction in fish, reducing the motility of the sperm and egg production. When used in high concentrations, like 10 μg/L, it is correlated with delayed hatching, skeletal malformations, and reduced survivability in zebrafish (S et al., 2024). Thus, it is important to find viable mechanisms and technologies to eliminate pharmaceutical drugs in the influent streams. Several techniques have been found to be effective in the removal of these substances, among which are biodegradation, photocatalytic degradation, nanofiltration, and membrane bioreactors; nevertheless, these approaches may prove to be expensive (J. F. Shaheen et al., 2024).

Adsorbents may be used as one of the promising methods of eliminating emerging micropollutants such as IBP. Literatures indicate the use of low-cost adsorbents, biochar and chitosan, that can be used to eliminate micropollutants in water (Mojiri et al., 2019). In that regard, the current study was devoted to the preparation of a new composite adsorbent consisting of Fe_3O_4 particles, Polyvinyl Alcohol (PVA), chitosan, and Spent Coffee Ground Biochar (SCGB) to adsorb IBP from aqueous solutions. PVA is also used in this composite as a protective layer to each Fe_3O_4 particles to prevent oxidation and as a cross-linking material between Fe_3O_4, SCGB and chitosan. The magnetite makes the composite easy to recover upon usage (Le et al., 2019), chitosan adds functional groups (Liakos et al., 2021) and SCGB makes the composite porous and of large surface area (Yang et al., 2025).

1.2. Problem Statement

Pharmaceutical contamination of aquatic systems is a great and increasing environmental issue of concern. It has been established in a number of studies that pharmaceuticals are capable of achieving toxic and detrimental effects on human health and aquatic ecosystems even at low

concentrations. The lack of biodegradability and high persistence and bioaccumulation of these substances increase these risks (Lessa et al., 2018; Rashid Ahmed et al., 2024). One of such pollutants is the anti-inflammatory medicine IBP, which is among the most commonly found pollutants of water (Zhang et al., 2024). The fact that the conventional WWTPs are not effective in eliminating these recalcitrant compounds is the continuous introduction of the medicines into the ecosystems, which contributes to their buildup and causes possible physiological and morphological changes in aquatic life (Rashid Ahmed et al., 2024).

Although developed treatment techniques have a potential, they are usually suppressed by the high costs and the production of secondary pollutants. On the other hand, adsorption provides a cost-effective, efficient, and viable way of eliminating dissolved pollutants in influent streams of WWTPs (J. F. Shaheen et al., 2024).

However, the gap in research in the creation of the eco-friendly, reusable, and inexpensive adsorbent, which is aligned with the ideas of the circular economy, is remarkable. SCGs, another important type of residual waste produced by the coffee industry, are a promising adsorbent material because they have a porous structure and adsorbing functional groups (Yang et al., 2025). Recent studies have shown that biochar can be improved in terms of performance by having chitosan, which is a natural biopolymer and has significant surface functional groups, such as hydroxyl (-OH), amino (-NH2), and carboxylic (-COOH), among others, which helps to improve performance by increasing adsorption efficiency (Sopanrao & Sreedhar, 2024).

PVA is also used as a serving polymer to increase the adsorption ability of the composite adsorbent in terms of mechanical strength and stability (Karaer Yağmur, 2020). Also, the introduction of magnetic particles (magnetite) enables the easy magnetic separation of the adsorbent and the treated water. The objective of the study is to formulate and define a magnetized biochar chitosan PVA composite that is based on SCGs. It will entail optimization of adsorption conditions to remove IBP as well as comprehensive isotherm and kinetic investigations to explain the adsorption process mechanisms, and finally attempt to develop a new ecologically friendly method of decontaminating water pollution by pharmaceutical agents.

1.3. Research objectives

1.3.1. General objective

The general objective of this research is to optimize selected operational parameters on the removal of IBP from aqueous solution using a magnetized SCGB-chitosan-PVA composite.

1.3.2. Specific objectives

The specific objectives of the study include:

- Synthesis and characterization of the magnetized SCGB-chitosan-PVA composite.
- Optimization of the adsorption process systematically by investigating the effects of key parameters such as pH, contact time, adsorbent dosage, and initial IBP concentration.
- Adsorption performance evaluation of Magnetized SCGB – Chitosan - Composite
- Long term stability and reusability Study of the composite for practical applications.

1.4. Significance of the Study

The study confronts the increasing problem of pharmaceutical contamination of rivers, lakes, and water systems with particular emphasis made on IBP and potential ways to provide a relatively cheap, yet environmentally friendly clean-up.

SCGB is used in solution with biodegradable polymers (chitosan and PVA) in creating a valuable resource; this helps in preventing more waste in landfills. Adding tiny particles of magnetite helps to speed up the adsorption and cause the pharmaceuticals to be attracted and then take the spent material out of the water simply by adding external magnet and hence reduces the amount of money used as well as the difficulty in disposing the waste.

These findings support global efforts to reduce pharmaceutical residues in waterways and provide a solid foundation for future research aimed at developing eco-friendly adsorbents for environmental engineering applications.

1.5. Scope of the Study

To achieve the aforementioned overall goals, the study's scope is addressed as follows. The adsorbent was prepared using chitosan, a derivative of chitin, which is the second most abundant natural material. SCGB was synthesized at different temperatures, and a chitosan/SCGB/PVA/magnetite composite was created through the impregnation method with

varying mixing proportions. Characterization of the materials included analyzing surface functional groups via FTIR, examining surface morphology with SEM, determining specific surface area using a surface area analyzer, and investigating the crystal and amorphous structures of SCG, SCGB, chitosan, magnetite, and the composite through XRD. The absorptive capacity of the composite for IBP removal was tested in a batch process. The interaction effects of parameters such as contact time, initial IBP concentration, adsorbent dosage, and initial solution pH were evaluated, followed by statistical optimization of removal efficiency using the RSM with a CCD. Additionally, the adsorption isotherm and kinetic rate as well as reusability of the adsorbent were investigated.

CHAPTER TWO

LITERATURE REVIEW

2.1. Water Pollution

Water, an essential resource for life on Earth, is one of the most vulnerable components of the environment. Consequently, water pollution has emerged as a critical global issue. Since the 3rd World Water Forum in Kyoto, Japan, in 2002, it has been reported that approximately 2 million tons of various pollutants, including sewage, industrial, and agricultural waste, are discharged into water bodies each day. This volume is nearly equivalent to the weight of the entire terrestrial population and leads to the generation of almost 1,500 km^3 of wastewater (Vasilachi et al., 2021).

Access to safe and reliable drinking water has become a significant concern for the global community, particularly in developing and underdeveloped countries. Approximately 800 million people worldwide lack access to potable water, with only 39% of the sub-Saharan African population and 46% of individuals in Oceania having reliable access (Yunusa et al., 2021). According to the 2021 World Water Development Report released by UNESCO, global freshwater use has increased sixfold over the past century, growing by about 1% per year since the 1980s. Alarmingly, over 80% of sewage generated by human activities is discharged into rivers and oceans untreated, resulting in environmental pollution and contributing to over 50 diseases. Poor water quality is associated with 80% of diseases and 50% of child deaths worldwide (Lin et al., 2022).

The primary causes of water pollution include the use of herbicides, fertilizers, pesticides, hazardous industrial chemicals, heavy metals, detergents, soaps, pathogens, textile dyes, and pharmaceutical compounds such as antibiotics and organic solvents, all of which contaminate water supplies (Kassahun et al., 2025). Among these contaminants, pharmaceuticals are frequently detected in various environmental compartments, underscoring the global concern regarding the removal of pharmaceutical micropollutants (Mojiri et al., 2019).

2.2. Pharmaceuticals

PPCPs are integral to daily life, comprising a diverse array of substances. This category includes medicinal compounds such as antimicrobials, anti-inflammatories, and lipid-regulating agents utilized in both human and veterinary medicine, as well as personal hygiene products like fragrances, disinfectants, and adjunctive agents. Pharmaceutical drugs are crucial for human health, animal care, agriculture, and aquaculture, primarily for disease treatment and prevention. Their consumption has been steadily increasing each year. However, interactions between active compounds and biological materials can result in unforeseen environmental consequences. Therapeutic compounds frequently enter aquatic systems from various sources, leading to the contamination of surface water with pharmaceutical substances and their metabolites (Eapen et al., 2024).

Pharmaceuticals have been detected in surface waters worldwide, with Addis Ababa, Ethiopia, being one notable location. The highest mean cumulative concentration was recorded in Lahore, Pakistan, at 70.8 µg/L, with a maximum concentration of 189 µg/L at one sampling site. La Paz, Bolivia, followed closely, with a mean concentration of 68.9 µg/L and a maximum of 297 µg/L, while Addis Ababa, Ethiopia, recorded a mean of 51.3 µg/L and a maximum of 74.2 µg/L. The most contaminated site was the Rio Seke in La Paz, Bolivia, which exhibited a cumulative API concentration of 297 µg/L (Pot E et al., 2022).

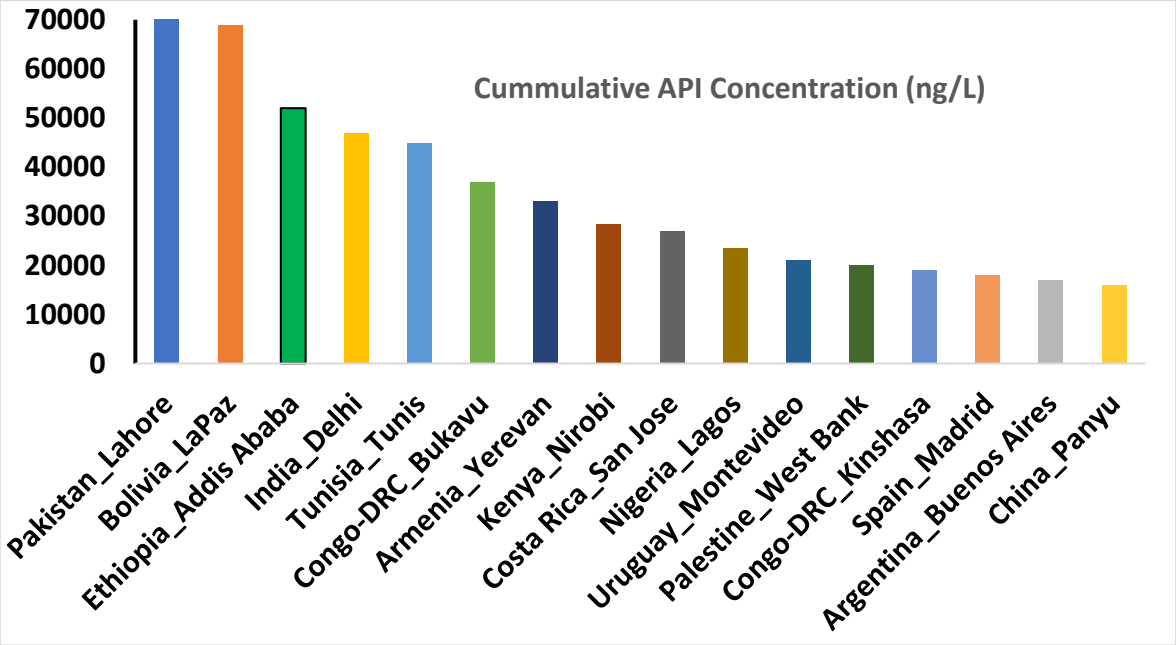

Figure 2.1: Cumulative API concentrations across different countries (Pot E et al., 2022)

2.3. Sources and Pathways of Pharmaceutical Pollutants into the Aquatic Environment

Aquatic systems serve as the main sinks for pharmaceutical contaminants. These contaminants mainly originate from pharmaceutical manufacturing, domestic sewage, healthcare facilities (including clinics and hospitals for both humans and animals), agricultural runoff, and stormwater from farms. Pharmaceuticals are used to improve human health, extend lifespans, and boost food production, which classifies them as human and veterinary drugs. When ingested, a typical human or animal absorbs about 20% of the drug, while around 80% is excreted through feces and urine. These excreted metabolites then enter sewage systems from domestic sources, CBDs, and healthcare facilities are eventually sent to WWTPs. Therefore, sewage from homes and health facilities is the main source of pharmaceutical residues in wastewater. Although treatment plants are crucial in removing pharmaceutical contaminants, their effectiveness can vary, sometimes leaving certain pharmaceuticals in the treated water that gets discharged into water bodies (Munzhelele et al., 2024).

2.4. Classifications of Pharmaceuticals

Pharmaceuticals are classified into various categories based on their mechanism of action, mode of action, chemical structures, and the diseases they address. When organized according to their therapeutic applications, they are referred to as therapeutic classes or groups. Examples of these classifications include analgesics, anti-inflammatories, antidepressants, antibiotics, antivirals, anticoagulants, and sedatives, among others. Table 2.1 presents key pharmaceutical contaminants, along with their corresponding chemical properties (Samal et al., 2022).

Table 2.1: Major Pharmaceutical pollutants

Sl. No.	Class/Group of Pharmaceutical	Pharmaceutical Contaminants	Formula	Mass (g mol^{-1})	pK_a	$logK_ow$
1	Analgesics and Anti-inflammatories	Aspirin	$C_9H_8O_4$	180	3.5	1.2
2		Diclofenac	$C_{14}H_{11}Cl_2NO_2$	296.2	4.91	4.51
3		IBP	$C_{13}H_{18}O_2$	206.3	4.15	4.51
4		Paracetamol	$C_8H_9NO_2$	151.2	9.38	0.46
5		Naproxen	$C_{14}H_{14}O_3$	230.3	4.15	3.18
Sl. No.	**Class/Group of Pharmaceutical**	**Pharmaceutical Contaminants**	**Formula**	**Mass (g mol^{-1})**	**pK_a**	**$logK_ow$**
1	Antibiotics	Sulfamethoxazole	$C_{10}H_{11}N_3O_3S$	253.279	5.6-5.7	0.89
2		Erythromycin	$C_{37}H_{67}NO_{13}$	733.93	8.88	2.48
3		Trimethoprim	$C_{14}H_{18}N_4O_3$	290.32	7.12	0.73

2.4.1. Analgesics and anti-inflammatories

Analgesics and anti-inflammatories are significant components of PPCPs present in wastewater. These heterogeneous substances are primarily utilized for pain relief and fever reduction. Analgesics can be classified according to their mechanisms of action into several categories, including paracetamol (acetaminophen), NSAIDs, opioids (such as morphine), cannabis (medical marijuana), alcohol, and cyclooxygenase-2 (COX-2) inhibitors. Commonly used analgesics and anti-inflammatories include diclofenac, IBP, and paracetamol, the latter of which is frequently administered to manage fever (Samal et al., 2022).

NSAIDs constitute a major category of pharmaceuticals extensively used to alleviate pain, reduce inflammation, and lower elevated body temperatures. They are commonly prescribed for conditions such as headaches, dysmenorrhea, sprains and strains, colds and flu, arthritis, and chronic pain. Despite their presence in negligible quantities (primarily in nanograms and micrograms) in various environmental matrices, including soil, wastewater, surface water, groundwater, sediments, snow, Antarctic ice, and drinking water, NSAIDs can exert prolonged ecotoxic effects on ecosystem biota. With over 30 million doses of NSAIDs consumed daily,

their usage is on the rise, underscoring the increasing importance of removing these pharmaceuticals from the environment (Banerjee & Maric, 2023; Samal et al., 2022).

The presence of NSAIDs in untreated water can lead to significant organ disorders in living organisms. Both invertebrates and vertebrates exposed to NSAIDs may experience oxidative stress, evident through changes in antioxidant enzyme activity (including catalase, superoxide dismutase, and glutathione S-transferase), alterations in total protein levels, and lipid peroxidation. The occurrence of diclofenac and ketoprofen has been associated with cardiovascular defects and cardiac anomalies in freshwater fish species such as Clarias gariepinus and Danio rerio. Moreover, NSAIDs can induce metabolic disturbances that affect detoxification enzyme activity, mitochondrial function, and membrane stability. They may also result in changes in gene expression, DNA damage, and endocrine disorders (Placova et al., 2023; Samal et al., 2022).

2.4.2. Antibiotics

Antimicrobial compounds that eliminate microorganisms and inhibit bacterial growth are referred to as antibiotics. These agents are crucial for the treatment of contagious diseases, the protection of human health, and the promotion of animal growth. Antibiotics facilitate protein synthesis and prevent bacterial proliferation. Over the past few decades, the demand for antibiotics has increased by 30%, positioning them among the most frequently prescribed pharmaceuticals. However, the presence of antibiotics in the environment raises significant concerns regarding the evolution and dissemination of antibiotic resistance genes, which have been classified as a global public health crisis (Samal et al., 2022).

The continuous introduction of antibiotics has resulted in their classification as pseudo-persistent compounds. Approximately 90% of antibiotics consumed by humans are excreted through urine or feces. These contaminants can enter the sewer system and, if not adequately treated, may pose risks to the ecosystem. Ground and surface water are also adversely affected by antibiotic use, becoming contaminated through leaching and agricultural runoff. Significant health risks associated with antibiotic use include cardiac arrhythmia, immune system disruption, liver dysfunction, bone marrow suppression, and detrimental impacts on the food chain (Samal et al., 2022; Tegegne et al., 2024).

2.4.3. Antidepressants

Neuroactive pharmaceutical compounds utilized for the treatment of anxiety and depression, management of addictions, and addressing chronic pain conditions are classified as antidepressants. Their presence in wastewater can pose significant health risks and other detrimental effects (Samal et al., 2022; Verhoeven et al., 2023).

2.5. Ibuprofen (IBP)

IBP is a drug that belongs to the group of NSAIDs (Mali et al., 2024). Remarkably, IBP is the third most prescribed and the second most produced NSAID globally (Ngernyen et al., 2023; Osman et al., 2024), and its annual production tops 20,000 tons (Ahmad, 2023; Chopra & Kumar, 2020). IBP is the most prescribed and widely researched of all the NSAIDs and has effects on its presence in aquatic environments. There are about 140 published articles, 75 percent of which examine NSAIDs in the environment with a major share on the use of IBP as the primary pollutant (J. F. Shaheen et al., 2024). Along with that, it features in the WHO Essential Drugs List (2010) (Chopra & Kumar, 2020) and is registered by the Ethiopian Food and Drug Authority. IBP is also widely recognized globally as an agent with anti-inflammatory effects used to treat fever, headache, musculoskeletal pain, menstrual pain, neurological pain, and post-surgical pain (as an antipyretic medication, analgesic medicine, and anti-inflammatory medication) (Chopra & Kumar, 2020; Jan-Roblero & Cruz-Maya, 2023).

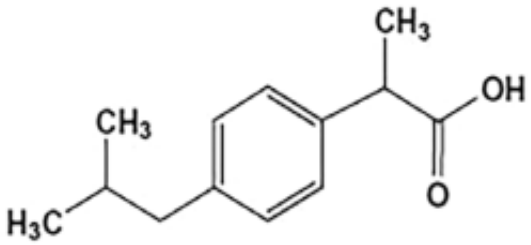

Figure 2.2: The structure of IBU

Table 2.2: Chemical and physical properties of IBU

IUPAC name	2-(4-(2-Methylpropyl)phenyl)propanoic acid
CAS number	15687-27-1
Molecular formula	C13H18O2
Molar mass	206.29 g/mol
Density	1.03 g/cm^3
Melting point	75 to 78 ˚C (167 to 172 ˚F)
Boiling point	157 ˚C (315 ˚F)
Solubility in water	0.021 mg/cm3 (20 ˚C)
pKa	4.52
log Kow	3.44

2.5.1. Sources and occurrence of Ibuprofen (IBP)

The anthropogenic activities would augment the levels of IBP in the environment by poor disposals, production sites, WWTPs, sewage treatment facilities and treatment of livestock. IBP is not metabolized completely after consumption and it is excreted releasing a number of metabolites that are even more toxic than the parent compound. After excretion, IBP and its derivatives may find their way to WWTPs, sewage treatment facilities, rivers, lakes, oceans, soil, and groundwater, and be absorbed by plants and aquatic fauna. Sewage treatment facilities and WWTPs are the main sources to monitor the level of IBP (Chopra & Kumar, 2020).

IBP is consistently detected in the effluent streams of WWTPs worldwide due to incomplete absorption after ingestion, leading to its release into the environment. The continuous detection of pharmaceuticals is attributed to their non-biodegradable nature and partial treatment at WWTPs (J. F. Shaheen et al., 2024). Concentrations of IBP have been recorded as high as 25 mg/L in WWTP effluents (Ahmad, 2023; da Silva et al., 2024). Metabolized IBP accumulates in natural matrices, primarily discharged into water systems, leading to accumulation in aquatic environments and soil. Non-consumed expired drugs often end up in household garbage, posing a risk of soil contamination. In veterinary medicine, IBP is also used, with excretion occurring in animal urine or feces (Jan-Roblero & Cruz-Maya, 2023). The therapeutic dosage of IBP ranges from 600 to 1200 mg/day, with approximately 15% excreted as unchanged molecules and their metabolites (Trianda et al., 2024).

Studies have reported NSAID concentrations ranging from 1.1 to 55 µg/L across Africa, with specific instances of 221 µg/L in South Africa and 1.4 µg/L in Turkey. Surface water contamination levels have been found to be 0.68 to 85 µg/L in Africa, 20 µg/L in Brazil, and 5.4 µg/L in China. Concerns regarding IBP in tap water include detected concentrations of 11–39 ng/L in Spain, 24–47 ng/L in Iran, 2.5–56 ng/L in France, 16 ng/L in Japan, and 8 ng/L in Sweden (Rashid Ahmed et al., 2024). IBP concentrations in wastewater have varied from 1.38 µg/L to 1673 µg/L in South Africa, Canada, and Pakistan, and from 0.004 µg/L to 603 µg/L in Bosnia and Herzegovina, Croatia, Greece, China, Korea, Switzerland, Sweden, Serbia, and the UK (J. F. Shaheen et al., 2024).

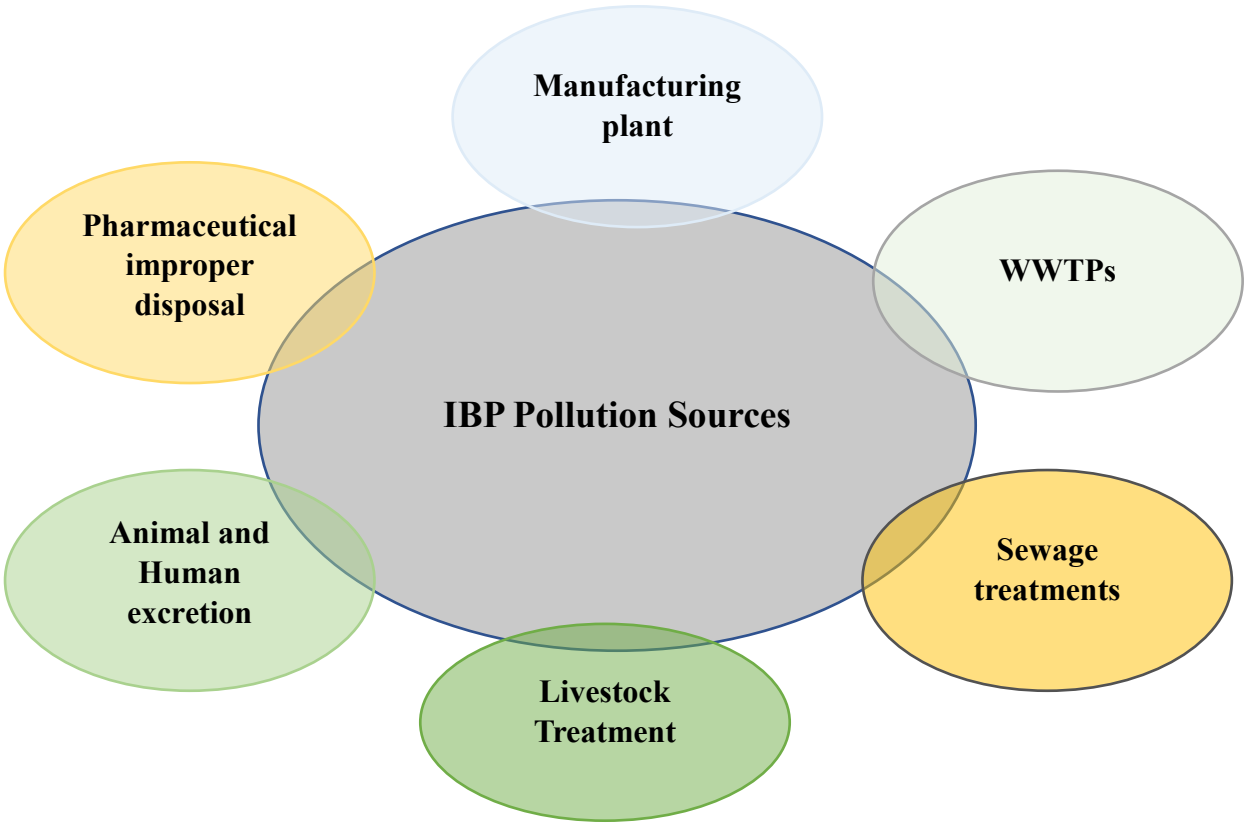

Figure 2.3: Sources and occurrence of IBP

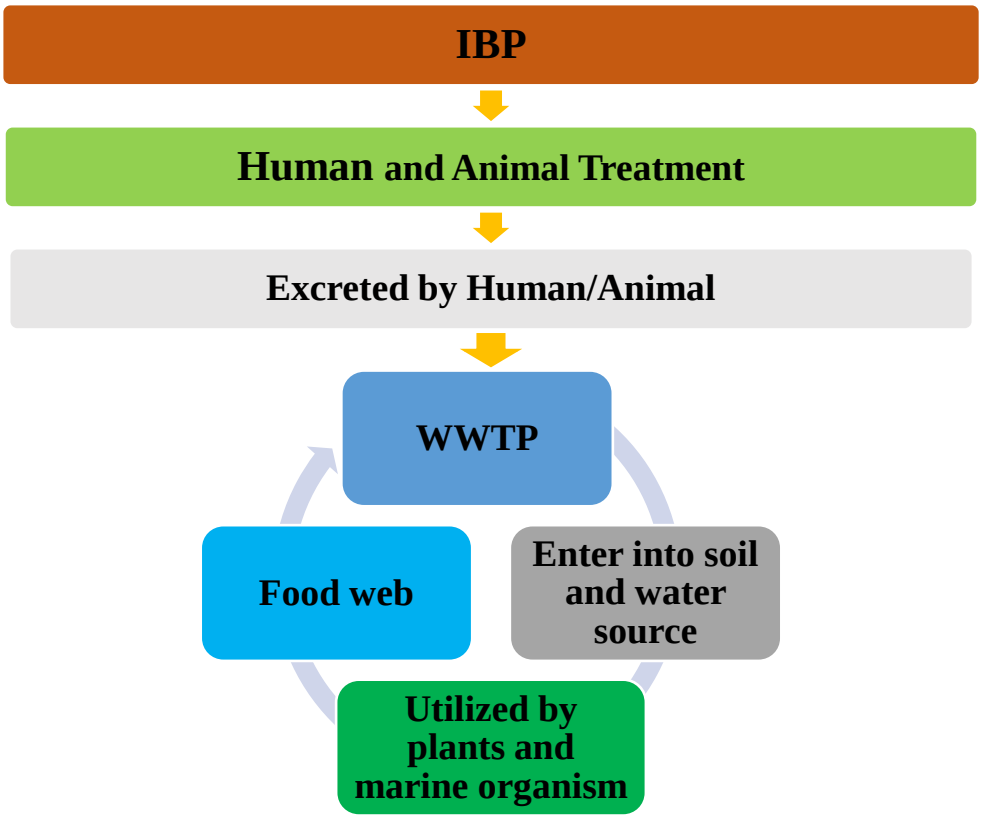

Figure 2.4: Pathway of IBP entering into food web

2.5.2. Health impacts and toxicity of Ibuprofen (IBP)

Despite its numerous advantages, IBP presents significant health and environmental risks. Concentrations of IBP in aquatic systems range from 18 to 6,297 ng/L and are deemed harmful to aquatic species (Kumar & Barakat, 2024). Research indicates that it decreases fish spawning. Additionally, concentrations between 1–100 ng/L of IBP have been associated with reduced activity in the amphipod crustacean Gammarus pulex (Chopra & Kumar, 2020). During the chlorination process, IBP in wastewater can transform into intermediate compounds with more toxic properties. Due to its physicochemical characteristics, IBP poses challenges for microbial degradation in the environment, potentially resulting in bioaccumulation and ecological damage (Trianda et al., 2024). The accumulation of IBP in drinking water may present health risks to humans, as it has been linked to adverse effects on the liver, kidneys, and gastrointestinal system. Some studies suggest that IBP and other pharmaceuticals may contribute to the development of antibiotic resistance in bacteria (Xing et al., 2023). Furthermore, the combination of IBP with other drugs may inhibit cell reproduction in human

embryos. Reports indicate that exposure to IBP can negatively impact the reproduction of aquatic vertebrates and has toxic effects on algae (Davarnejad et al., 2018).

Studies have demonstrated that the presence of IBP at concentrations up to 12 μg/L in aquatic environments can lead to alterations in oxidative stress in the brain and gut tissue of zebrafish (J. F. Shaheen et al., 2024).

2.6. Ibuprofen (IBP) Removal Methods from Aqueous Solutions

Various advanced techniques are employed for the removal of PPCPs, including adsorption methods such as powdered activated carbon and granular activated carbon, biofiltration techniques (trickling filters, sand filters, biological activated carbon filters, etc.), reverse osmosis, attached growth technology, membrane bioreactors, nanofiltration, carbon nanocomposites, and magnetic nanoparticles ($CoFe_2O_4$). These methods remain in the developmental phase, with numerous opportunities for further research. However, the absence of optimal treatment methods has led to the release of various pollutants, including PPCPs, pesticides, and hydrocarbons, along with their metabolites into the environment (Chopra & Kumar, 2020).

To mitigate the adverse effects of IBP, several remediation techniques have been developed and evaluated for their effectiveness. Water treatment technologies aimed at removing, containing, or reducing IBP in wastewater can be categorized into three groups: chemical, physical, and biological methods. Various approaches have been utilized, including advanced oxidation processes, membrane separation, extraction, biodegradation, coagulation, and adsorption. It is important to note that while each method possesses unique benefits, many can be complex, require high maintenance and investment costs, and generate harmful sludge (Lekene et al., 2023).

Among these treatment methods, adsorption has garnered significant attention due to its advantages in removing PPCPs. It offers simplicity, potential efficiency, high selectivity at the molecular level, low investment costs, low energy consumption, minimal secondary pollution, and good reversibility (Osman et al., 2024). The adsorption method has attracted considerable interest from researchers as a promising mechanism for the removal of IBP. The efficiency of adsorption primarily depends on the properties of the adsorbent material, including specific surface area, cost, eco-friendliness, porosity, selectivity, reusability, and crystal structure

(Lessa et al., 2018; Murtaza et al., 2022). Due to its high efficiency, low operational and maintenance costs, straightforward design, low initial expenses, and the availability of a wide range of adsorbent materials, adsorption has become a widely adopted treatment mechanism (Khierallah et al., 2021).

2.7. Adsorption

Adsorption is the process of adhering an adsorbate (solute) from a different form (a gas or a liquid solution) to an adsorbent (solid surface) by the aid of chemical or physical drags. The technique has been mostly useful in removing organic and inorganic pollutants in water and wastewater treatment. The process of adsorption depends on a number of factors, particularly those related to IBP. Most science contains factors such as the duration of contact, the initial pH of the effluent, dosage of the adsorbent, and initial concentration of IBP. In recent times, several scholars have focused on adsorption mechanisms, which have been found to be the most effective treatment mechanisms. The United States Environmental Protection Agency affirms that adsorption offers low operating expenses, high efficiency of the removal, fast rate of reaction, and simple working design (Singh et al., 2023). The effective removal of IBP in water and wastewater using various biomass-based adsorbent materials had been mixed and used.

2.7.1. Physical adsorption

Following physical adsorbent occurs when low level intermolecular forces bind both the adsorbent and the adsorbate. In the process, the adsorbent and adsorbate molecules are brought into contact with each other via van der Waals and intermolecular dipole-dipole forces, possibly involving hydrogen bonding. In addition, physical adsorption is reversible (Mahmood Aljamali & Obaid Alfatlawi, 2021).

2.7.2. Chemical adsorption

In chemical adsorption the adsorbent and adsorbate are held together by strong chemical bonds, normally ionic or covalent. Such a strong interaction makes chemical adsorption irreversible. In contrast to the physical adsorption, the example of the chemical adsorption is the creation of a monomolecular overlay of the adsorbate on the surface of the adsorbent. (Mahmood Aljamali & Obaid Alfatlawi, 2021).

2.8. Factors Affecting Adsorption Process

2.8.1. Initial Ibuprofen concentration

The initial concentration of IBP greatly affects the elimination of IBP in the solution. The relationship that exists between the starting concentration of an adsorbate and the presence of active sites on the surface of the adsorbent determines the removal efficiency. Particularly, the effect of initial IBP concentration on the composite removal efficiency is proportional to the number of IBP molecules in solution to the number of the active adsorption sites. Normally, the higher the concentration of IBP, the lower the percentage of the removal. This decrease is explained by the increased concentration of IBP causing a low number of free binding sites of the adsorbent (Ahmad, 2023).

2.8.2. pH

The pH effects on IBP adsorption with biochar have been studied by many researchers and provided important information on the mechanism and effectiveness of adsorption. Other studies suggest that the decreased pH rates tend to increase the adsorption of IBP on the biochar surfaces. This increase is the product of greater protonation of the biochar, which increases the electrostatic interactions with negatively charged IBP molecules. This protonation enhances the number of positive charges on the biochar, thus, enhancing its ability to attract and retain IBP which eventually results in excellent adsorption performance. Also, studies demonstrate a great influence of the adsorption of biochar on IBP by the pH in which the material adsorbs better under acidic environments. However, at lower pH more active sites on the biochar surface are exposed which eventually increase the interaction of IBP with the biochar. On the other hand, an increase in the pH causes the deprotonation of IBP molecules, which makes them less affined with biochar causing a decline in the adsorption efficiency. Research indicates that the higher the levels of pH, the lower the sorption capacities of IBP (Rashid Ahmed et al., 2024).

2.8.3. Contact time

Contact time between the adsorbent and the adsorbate is also important in the adsorption process. The rate at which the adsorbent material can be taken up and the time also shows how the share should be shorter as a sign of its effectiveness (Shin et al., 2021). According to literatures, the adsorption rate is high initially which is mainly because of the number of free active sites on the adsorbent that are many initially. Nevertheless, towards equilibrium, the rate

of adsorption reduces. Such a decrease in uptake in equilibrium is explained by the fact that there is a small number of active sites that allow further adsorption (Yeliz Ozudogru & Ecem Tekne, 2023).

2.8.4. Adsorbent dosage

The effect of different concentrations of biochar on adsorbing IBP in wastewater has been studied by many researchers, which have offered an insight into the mechanism and effectiveness behind the adsorption process. Through research studies, it has been established that the adsorption capacity increases substantially as the dosage of biochar increases. as the dosage of biochar decreases in concentration, the efficiency of the adsorption process also decreases. It is explained by the fact that more active sites of the biochar surface are available, and the interactions with the molecules of IBP become more efficient (Rashid Ahmed et al., 2024).

2.9. Spent Coffee Ground (SCG)

Coffee is a valuable commodity in the world (Sunyoto et al., 2022). Coffee farming originated in Ethiopia's highlands during the 9th century and gained popularity as a beverage in the Arab world by the 15th century. It subsequently spread to regions such as Yemen, Turkey, and Europe. Today, coffee is the second-most traded agricultural commodity worldwide, following oil, with an estimated export value of USD 36.3 billion in 2021. Over recent decades, coffee consumption has surged due to urbanization, the growth of coffee culture, and changing consumer preferences, which have placed considerable pressure on coffee production systems (Tsigkou et al., 2025).

Ethiopia is renowned for its Arabica coffee, with an estimated total production of 8.35 million 60 kg bags (501,000 MT) for the 2023/24 season. The coffee industry plays a vital role in Ethiopia's economy, as well as its sociocultural and spiritual life. However, coffee production faces environmental challenges, particularly concerning the management of coffee processing waste (Kassahun et al., 2025). As the birthplace of Arabica coffee genetic diversity, Ethiopia is the largest producer and consumer of coffee in Africa, generating 30–35% of its total export earnings from this crop (Tsigkou et al., 2025).

SCGs are a primary by-product of soluble coffee processing (Singh et al., 2023). Globally, SCGs are recognized as one of the most common forms of biomass waste, with sources

categorized as domestic, commercial, and industrial. Unfortunately, landfills are often the final destination for most SCGs. This results in anaerobic decomposition, which produces and releases potent greenhouse gases. Consequently, researchers worldwide are exploring a variety of potential uses for discarded coffee grounds and their by-products, including biofuels, adsorbents, catalysts, cosmetics, composite materials, animal feed, and more. SCGs are rich in carbohydrates, lipids, proteins, and minerals, making them a focus of research for diverse applications (Saxena et al., 2024).

2.9.1. Spent coffee ground biochar (SCGB)

Biochar is a type of material composed of carbon and is produced by a three-stage process known as controlled pyrolysis of biomass and is conducted in low oxygen environment. The products of this process are a functional substance on which the functional chemical groups of their composition can be located, which allows effective interaction with organic and inorganic compounds (Oliveira et al., 2021).

SCG, a worldwide waste product with a vast concentration, can be transformed to SCGB, which presents a prospective solution owing to its large surface area, porous makeup and cost-effectiveness earned through its carbonaceous content of its pyrolysis product (Nagarajan et al., 2024). The kind of feedstock that is utilized and the conditions under which it is pyrolyzed affect the properties of biochar which comprises of its chemical composition, surface area, and structure. Pyrolysis temperature plays a pivotal role in defining the properties of the products of biochar (Rashid Ahmed et al., 2024). The huge quantities of food waste that are deposited in the municipal sewage systems are a major threat to the social environment. Landfills that handle food waste lead to the production of high amounts of methane, chlorofluorocarbons, and carbon dioxide. The increasing environmental consciousness has created an interest on the use of food waste materials as well as agricultural by-products to form biochar. When converted into biochar, biowaste coffee grounds are a promising and relatively cheap adsorbent, and have been explored to assess their ability to remove pollutants of aqueous solutions (Zungu et al., 2022).

2.10. Chitosan

Chitosan is a biopolymer that is synthesized by an approach of deacetylation of the natural polysaccharide chitin, which is found in great quantities. It finds application in different processes such as in the process of eliminating pollutants. Chitosan is easy to alter and mold in

various shapes and sizes. In comparison to commercial adsorbent materials, chitosan has a number of benefits, which include low cost, being eco-friendly, having a macromolecular structure, and high adsorption capacity. Past studies have established that chitosan is a useful biopolymer when it comes to extracting IBP in synthetic aqueous solutions (Kumar & Barakat, 2024). These functional groups are active sites, which facilitate the affinity of chitosan on a variety of organic and inorganic contaminants since the chitosan contains the amino, primary, and secondary hydroxyl groups. Moreover, the characteristics of chitosan, including high porosity, biocompatibility, biodegradability, low production of toxic by-products, and more, have created a lot of interest in chitosan as an adsorbent in many sectors (Aranaz et al., 2021).

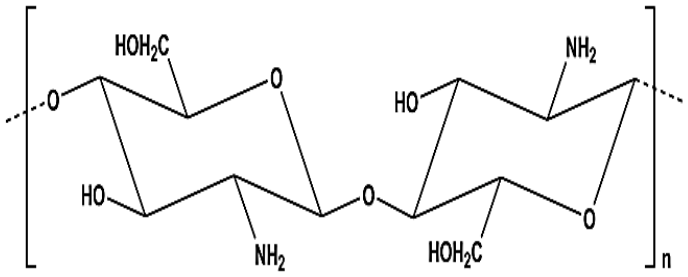

Figure 2.5: Structure of Chitosan

2.11. Polyvinyl Alcohol (PVA)

Polyvinyl Alcohol (PVA) is a fairly inexpensive, non-toxic, water-soluble synthetic polymer with high-interest in artificial polymers because of favourable physicochemical and viscoelastic characteristics. It gives rise to a wide range of different biomedical applications, including wound dressings and tissue engineering, due to biodegradable and biocompatible properties (Karaer Yağmur, 2020). Moreover, PVA acts as a protective layer and encases every particle of Fe_3O_4 to prevent oxidation and serve as a cross-linking solution between Fe_3O_4, SCGB, and Chitosan (Le et al., 2019).

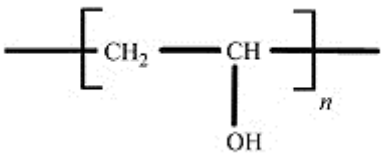

Figure 2.6: Structure of PVA

2.12. Magnetite

The use of magnetite particles (Fe_3O_4) has become highly visited research in the field of materials science and technology because of its characteristics of magnetic properties, biocompatibility, and various potential applications in biomedical technology, electronics, and environmental studies (Mardana & Arjana, 2024).

They are also easily modified and manipulated which increases their applicability in many sectors including using it in the medical world as well as environmental solutions. In particular, they are very efficient in the treatment of water and the removal of pollutants, which is explained by their capacity to adsorb and affix dangerous agents (Mardana & Arjana, 2024). However, one of the greatest obstacles which has delayed the use of SCGs in industries is that it is difficult to recover and reuse them after adsorption. This problem can be addressed by use of magnetic separation technology which is a simple and effective technique of isolating the powdered adsorbents and the target pollutants of the aqueous phase in the external magnetic field. Fe_3O_4 is also one of the crucial elements in this respect as the part of the adsorbents (Le et al., 2019).

2.13. Summary of Previous Studies on the Removal of IBP

There has been a wide range of literature addressing the process of adsorption of IBP from wastewater using diverse adsorbents, as well as under various operating conditions. In one of the studies, the adsorption of IBP was optimized using biochar and magnetic biochar made using chrysanthemum waste in the beverage sector. The study compared in the contact time (5-180 minutes) and pH of the solution (2-12) and the initial drug concentration (5-100 mg/L). It took one hour to reach equilibrium, and maximally IBP was removed at pH 2 in the case of biochar and at pH 4 in the case of magnetic biochar. The kinetics of adsorption were measured against the models of PFO, PSO, and IPD rate, whereas the adsorption equilibrium was measured according to Langmuir, Freundlich and the Langmuir-Freundlich isotherm models. The findings suggested that PSO order kinetic model and the Langmuir-Freundlich isotherm model best characterized the adsorption kinetics and isotherm of both forms of biochar with the largest adsorption capacities of 167 mg/g and 140 mg/g in biochar and magnetic biochar respectively (Ngernyen et al., 2023). The other study was based on a cross-linked aerogel adsorbent made of chitosan that had a particular surface area of 1020 m^2/g and a pore size of

45 to 150 μm. The adsorption equilibrium was well described with the help of the Langmuir model because the maximum capacity was obtained at 596 mg/g at 25 °C (da Silva et al., 2024). Also, studies on modified date palm biochar reported an IBP adsorption capacity of 72.2 mg/g when optimal conditions were taken (pH 2, concentration 150 mg /L, time 20 hours) (S. M. Shaheen et al., 2022). A different study on IBP-COF indicated a high level of adsorption performance as the equilibrium was established after 60 minutes and a capacity of 512 mg/g, which is better than the traditional adsorbents. Its kinetics were correlated with PSO and Langmuir models, and it is a sign of efficient monolayer adsorption (AlNeyadi et al., 2024). Moreover, carbon-based adsorbents have also been studied, but the results demonstrated a big range of differences between adsorption of IBP, with the activated carbon showing a range between 10.8 and 408 mg/g, and biochar being between 2.5 and 1033 mg/g (Osman et al., 2024). According to the reviewed literatures, the key issues affecting the adsorption process are the initial pH of solution, adsorption time, dosage of adsorbent and initial concentration of IBP.

CHAPTER THREE

MATERIALS AND METHODS

3.1. Chemicals and Equipment

3.1.1. Chemicals and reagents

All chemicals used in this study were of analytical grade and used without further purification. Ferric chloride, ferrous chloride, and sodium hydroxide (NaOH) were employed to prepare magnetite (Fe_3O_4) via the co-precipitation method. Acetic acid (1.5%) and PVA (1,500) were used to dissolve and cross-link chitosan during the preparation of the chitosan/SCGB composite. Chitosan derived from shrimp shells (75% deacetylated) and SCGB were combined to create a chitosan/SCGB composite adsorbent through impregnation. Magnetite was incorporated into the preparation of the magnetic SCGB-chitosan composite. Sodium hydroxide (99.9% purity) and hydrochloric acid (35%) were used to adjust the pH during the investigation of pH effects. IBP ($C_{13}H_{18}O_2$) was used to prepare various working concentrations, with distilled water and ethanol serving as solvents.

3.1.2. Apparatus and equipment

The following apparatus and equipment were utilized in this study. A magnetic stirrer was used to mix the solution during the adsorption process. The UV-visible spectrophotometer measured absorbance and IBP concentration. A 0.2 μm syringe filter was employed to separate the magnetic SCGB-chitosan composite from the mother liquor. Additional instruments, including an analytical balance, oven, furnace, ultrasonicate, overhead mixer, water bath, pH meter, beaker, dryer, mortar, and sieve, were also used throughout the study.

The surface morphology of the adsorbent was examined using a SEM. FTIR was employed to identify the functional groups of SCGB (carbonized at different temperatures) and the magnetic SCGB-chitosan-PVA composite (prepared at different ratios of SCGB and chitosan). XRD analysed the crystal structure of these materials. A BET surface area analyzer measured surface area.

3.2. Raw Material Treatment and Sample Preparation

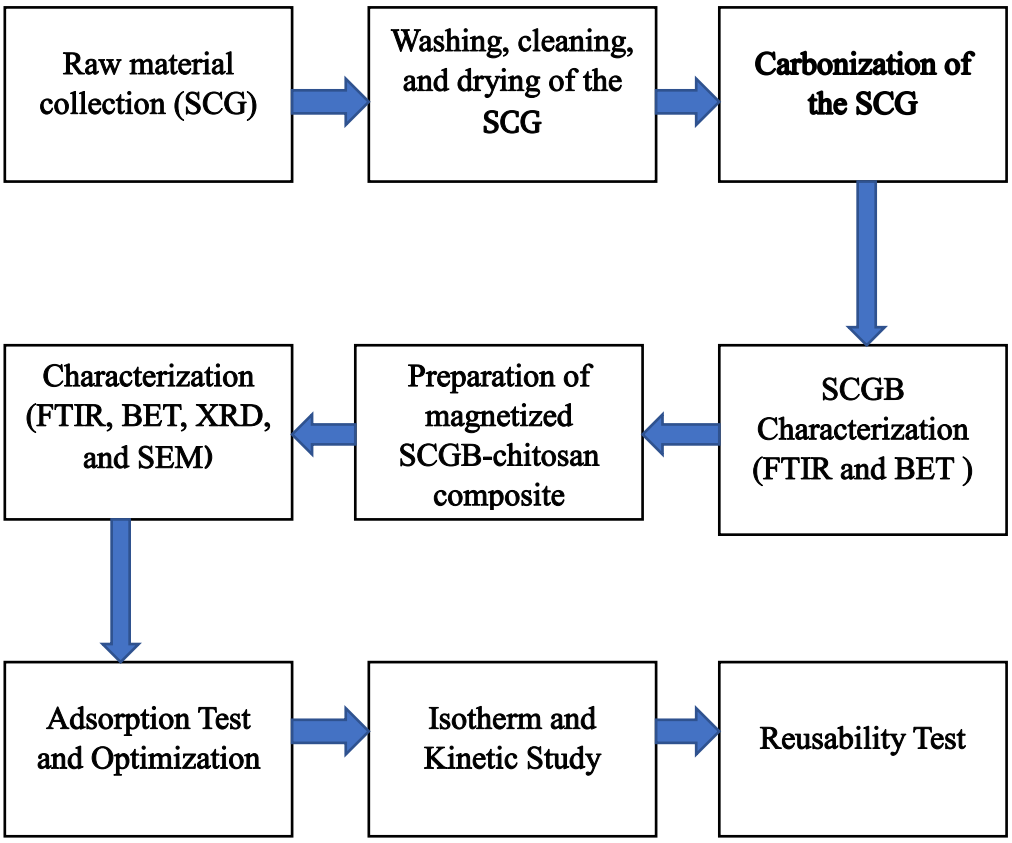

Figure 3.1: Process flow diagram of the experimental work

3.2.1. Raw material collection

The ingredients on which the synthesis of the magnetized SCGB-chitosan composite adsorbent is to be carried out were obtained at the local level in Addis Ababa, Ethiopia. These ingredients were chitosan (degree of deacetylation 75%), ferric chloride, ferrous chloride, PVA (degree of polymerization 1,500), IBP, SCG and acetic acid (1.5%).

3.3. Spent Coffee Ground (SCG) Characterization

3.3.1. Proximate analysis of spent coffee ground (SCG)

Spent Coffee Grounds (SCGs) were analysed for their physical and chemical characteristics using methods from the ASTM. The moisture content was determined according to ASTM D2867, and the ash content was assessed using ASTM D2866-94 (Kassahun et al., 2025).

3.3.1.1. Moisture content

3 g of SCG was taken, weighed, and dried in an oven at 105 °C for 24 hours. The sample was reweighed at varying intervals of 24 hours until a constant weight (W1) was achieved. The moisture content was determined using equation (3.1) (Jeníček et al., 2022).

$$MC = \frac{W_0 - W_1}{W_0} \times 100 \quad \text{.....(3.1)}$$

Where, MC = moisture content, W_1 the weight of SCG received from the oven and W_0 is the initial weight of SCG

3.3.1.2. Ash content

A muffle furnace was used to determine the ash content. The sample (3-gram) was put in a pre-weighed crucible and the content incinerated at 550 °C for 6 hours until ash was completely formed. The crucible was incinerated, then cooled to room temperature using a desiccator. Following the above, the weight of the ash was obtained, and the ash content was obtained by dividing the Equation (3.2) (Inayat et al., 2022).

$$AC = \frac{W_{ash}}{W_O} \quad \text{.....(3.2)}$$

Where, AC = ash content, W_0 = the initial weight of the sample before thermal decomposition, W_{ash}= the weight of the sample after thermal decomposition.

3.4. Synthesis of Spent Coffee Ground Biochar (SCGB)

SCG were gathered from coffee houses and then washed using ethanol and water, dried, and then processed. SCG was loaded into crucibles until they were full and covered with foil then subjected to carbonization in a muffle furnace with a limited supply of oxygen (de Souza et al., 2022;Yang et al., 2025). It was heated and allowed to pyrolyze at different final temperatures of 500, 550, and 600 °C. Each temperature of the carbonization process took 2 hours. The samples of biochar produced by SCG were also marked in relation to the temperature of carbonization (e.g. BC500 to biochar produced at 500 °C). The equation was used to compute the yield percentages of the end product with each pyrolysis temperature (Lekene et al., 2023):

$$\text{Mass yield}(\%) = \frac{\text{Mass of obtained biochar (g)}}{\text{Mass of raw material (g)}} * 100\% \quad \text{.....(3.3)}$$

3.5. Preparation of Magnetite (Fe_3O_4)

The reagents used for the synthesis included ferric chloride ($FeCl_3 \cdot 6H_2O$) and ferrous chloride ($FeCl_2 \cdot 4H_2O$) salts in a molar ratio of 1:2, along with NaOH, HCl, and ethanol. All materials were used without prior purification, with deionized water serving as the solvent. Two mixtures were prepared by combining 1 mL of 2M $FeCl_2 \cdot 4H_2O$ and 4 mL of 1M $FeCl_3 \cdot 6H_2O$, which were mechanically stirred at 1000 rpm for 3 minutes. Following this, 25 mL of 1M NaOH solution was added dropwise to the mixture, resulting in an immediate color change to black, indicative of magnetite. To neutralize the anionic charge on the magnetic particle surfaces, 0.5 mL of 2M hydrochloric acid (HCl) was added. The pH of the solution was monitored during the addition of NaOH. The reactants were magnetically stirred throughout the precipitation process, during which the pH level decreased from 12 to 8 using HCl and stirring for 2 hours at 40°C. The precipitates were washed twice with deionized distilled water and then with ethanol to remove impurities. To separate the supernatant liquids (ethanol and water), the mixtures were centrifuged, and the supernatants were decanted. Centrifugation continued until thick black precipitates remained. Finally, the precipitates were dried at 80°C for 24 hours and ground into a fine powder, preparing them for further analysis (Dehghanpour, 2020).

3.6. Preparation of Magnetized SCGB-Chitosan Composite

Magnetized SCGB-Chitosan Composite was prepared by the following means. The solvent casting technique was used to prepare the magnetized SCGB-Chitosan composites with different weight ratios such as; SCGB: Chitosan = 75: 25, 50:50, and 25:75 and the weight of the magnetite and PVA retained the same weight values. To start with, 3.5 g of Chitosan was thoroughly dissolved in 120 mL of 1.5 v/v-% acetic acid solution. A Chitosan solution was stirred with a solution of PVA prepared by dissolving 3g of PVA in 120 mL of distilled water. Chitosan-PVA mixture was stirred at room temperature and mixed under the magnetic stirring for 30 minutes and 10.5 g of SCGB was added to the mixture. Then, 3 g of magnetite was suspended in 20 mL of distilled water and sonicated within 15 minutes then added into the mixture. This was now thoroughly blended with the help of an overhead mixer and sonicated in ultrasonic bath further 30 minutes. The filmogenic solution thus obtained was poured carefully into an 85 x 10 mm Petri dish. Following the solvent-casting step, the Petri dish of

the magnetized SCGB-Chitosan composite was taken out, washed with distilled water, dried overnight at 40 ^{o}C in the oven, and placed in a desiccator (Lessa et al., 2018). The rest of SCGB to Chitosan ratios were also prepared in the same way.

Table 3.1: Preparation and sample codes for the biochars and composites

Sample	Treatment Temperature (^{o}C)	Treatment duration (Hour)	Impregnation Ratio (Biochar:Chitosan)	Sample Code
Biochar	500	2	-	BC500
Biochar	550	2	-	BC550
Biochar	600	2	-	BC600
Composite	-	1	75:25	Composite (75:25)
Composite	-	1	50:50	Composite (50:50)
Composite	-	1	25:75	Composite (25:75)

3.7. Physicochemical characterization of magnetized SCGB-Chitosan composite

The physico-chemical characterization of the SCG, SCGB, and the magnetized composite of SCGB-chitosan involved using different methods. FTIR analysis was used to analyze surface functional groups. SEM was applied to understand surface morphology. Specific surface area was calculated BET. XRD was used to determine the crystal structure of adsorbent materials.

3.7.1. Specific surface area characterization

The BET method was used to estimate the specific surface area of the SCGB, magnetite, and a magnetized spent coffee ground-chitosan composite, and it uses the adsorption and desorption of nitrogen gas at room temperature and 760 mmHg to determine the sample surface area. Initially, the empty tube was put to measure then 0.05 g of sample was put in it and weighed. The sample was then allowed to pump, 300 °C, 8 hours in order to eliminate water and volatile substances. The tubes were set into the micrometric machine, and the liquid nitrogen was also

added into the two flasks and was put in the surface area analyzer. Nitrogen gas adsorption and desorption isotherm in 77 K and 760 mmHg were used to determine the specific surface area of the surface (Sopanrao & Sreedhar, 2024).

3.7.2. XRD analysis

XRD is a non-destructive method of analyzing the crystallinity structure. XRD was done to establish whether the prepared composite was crystalline or amorphous. Miners are made up of minerals that have a characteristic X-ray diffraction. The range of diffraction angle, 2theta, ranged between 0 degrees and 80 degrees (Zuluaga et al., 2024).

$$n\partial = 2d\sin\theta \quad \text{.....(3.4)}$$

Where n is an integer, ∂ is the wavelength of the X-ray d is the inter-planar spacing generating the diffraction, and θ is the diffraction angle (Omidvar-motlagh et al., 2023).

3.7.3. FTIR analysis

FTIR spectroscopy determines chemical bonds of a molecule in wavelength 4000 to 400 cm^{-1}. It produces an infrared absorption spectrum which forms a molecular fingerprint, where the frequencies which are absorbed in an infrared spectrum give the vibrational energies of the atomic bonds. Functional groups FTIR spectra of the 4000-500 cm^{-1} range characterized the functional groups of BC500, BC550, BC600, composite (75:25), composite (50:50), and composite (25:75) in the PerkinElmer FTIR machine. The detector was brought close to the sample and infrared radiation of monochromatic wavelength was emitted in the source. A splitter was made with a partial mirror upon which some radiation escaped and the remainder was reflected when the infrared light got to the splitter. The two created beams were sent to a mirror, which was reflected to the splitter. At the splitter, the beams were once more split with one portion of the radiation returning to the sample and entering the detector and the other bouncing off the mirror and having to go back to the source of radiations (Dima et al., 2023).

3.7.4. SEM analysis

SEM is critical to the investigation of the surface morphology of adsorbent materials, which gives the information about its shape and structure (Yusmaniar et al., 2023). In this study, the SEM analysis of the composite was done in South Korea.

3.8. Preparation of Adsorbate Solution

A standard IBP stock solution was prepared by dissolving 30 mg of IBP in 1 L of distilled water and ethanol (10% of the liquid is ethanol), resulting in a concentration of 30 mg/L. Other concentrations (1 mg/L, 3 mg/L, 6 mg/L, 9 mg/L, 12 mg/L, and 15 mg/L) were achieved by diluting this stock solution. The absorbance of each diluted concentration of IBP was measured using a UV-vis spectrophotometer at 222 nm. A calibration curve was created by plotting concentrations against absorbance values, exhibiting a correlation coefficient (R^2) of 0.9949.

Table 3.2: Absorbance value of IBP concentration at 222 nm

Concentration (mg/L)	Absorbance
1	0.0117471
3	0.0290494
6	0.0532562
9	0.0755233
12	0.093169
15	0.111972

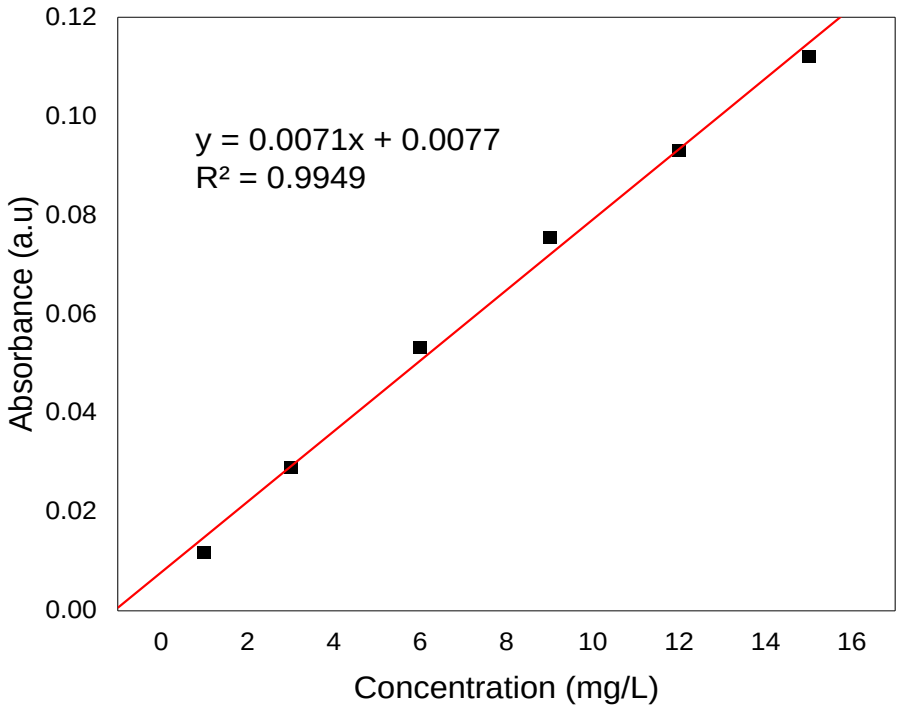

Figure 3.2: Calibration curve for IBP

3.9. Adsorption Experiment

The adsorption of IBP onto a composite (75:25) was conducted with 60 mL of solution, which was magnetically stirred for a predetermined duration. At the end of each batch adsorption experiment, aliquots were taken from the reactor and filtered using a 0.2 µm syringe filter. The absorbance of the filtrate was measured using a UV-vis spectrophotometer at 222 nm. The concentrations of each filtrate were determined by measuring their absorbance. and applying them to the standard curve equation. The percentage of IBP removal was calculated using equation (3.5).

$$\% \text{ Removal Efficiency} = \left(\frac{C_i - C_f}{C_i}\right) \times 100 \quad \text{.....(3.5)}$$

Where C_i and C_f are the initial and final IBP concentration in (mg/L) respectively. All experiments were conducted according to the experimental layout (Egbedina et al., 2023).

3.10. Study of Interaction Effect of Process Parameters and Model Evaluation using Central-Composite Design Response Surface Method

The adsorption of IBP using a magnetized SCGB-chitosan composite adsorbent was conducted in a batch process. The four key factors affecting IBP adsorption are: contact time, solution pH, initial IBP concentration, and adsorbent dosage. Based on the one-factor-at-a-time data, the following ranges were selected for further study: contact time (20-100 minutes), initial IBP concentration (2.5-12.5 mg/L), adsorbent dosage (0.5-2.5 g/L), and solution pH (2-10), with three levels for each parameter.

The interaction effects among these parameters were examined using the CCD, a subset of RSM. This approach identified the optimal process parameters for effective IBP removal using the adsorbent material. The removal efficiency was modeled with the independent variables through a quadratic regression equation.

3.11. Independent Factors and their Coded Levels for CCD Experiments

Table 3.3: Independent factors and their coded level for CCD experiment

Factor	**Symbol**	**Units**	**Levels**		
			Low (-1)	Medium (0)	High (+1)
pH	A	-	2	6	10
Initial Conc. of IBP	B	mg/L	2.5	7.5	12.5
Adsorbent Dosage	C	g/L	0.5	1.5	2.5
Contact time	D	min	20	60	100

This study investigated the interaction between key process variables contact time, initial concentration of IBP, adsorbent dosage, and solution pH to establish a mathematical relationship between the independent and dependent variables.

Experimental setup

Table 3.4: CCD design matrix for four factors

	Factor 1	Factor 2	Factor 3	Factor 4	Removal efficiency (%)
Run	**A: pH**	**B: concentration (mg/L)**	**C: dosage (g/L)**	**D: time (min)**	
1	4	5	2	80	*
2	4	10	2	40	*
3	4	5	1	80	*
4	6	2.5	1.5	60	*
5	8	10	1	40	*
6	6	12.5	1.5	60	*
7	6	7.5	1.5	60	*
8	6	7.5	0.5	60	*
9	6	7.5	2.5	60	*
10	4	10	1	80	*
11	4	10	1	40	*
12	8	5	1	40	*
13	6	7.5	1.5	60	*
14	6	7.5	1.5	20	*
15	10	7.5	1.5	60	*
16	4	5	1	40	*
17	8	5	2	40	*
18	8	10	2	40	*
19	4	5	2	40	*
20	8	5	1	80	*
21	6	7.5	1.5	100	*
22	8	10	2	80	*
23	6	7.5	1.5	60	*
24	4	10	2	80	*
25	2	7.5	1.5	60	*
26	6	7.5	1.5	60	*
27	8	10	1	80	*
28	6	7.5	1.5	60	*
29	6	7.5	1.5	60	*
30	8	5	2	80	*

The removal efficiency obtained from the experimental investigation, which considered the interaction effects of the four operational parameters, was analyzed. The model's significance was evaluated using a statistical tool (ANOVA), focusing on the coefficient of determination

(R^2), F-value, and p-value. Three replicate experiments were conducted, and an average value was computed.

3.12. Optimization of Process Parameters and Statistical Analysis

The optimization of process variables contact time, initial concentration of IBP, adsorbent dosage, and initial solution pH was conducted using Design Expert version 13. The removal efficiency from an experimental study of these four parameters served as the response variable. Triplicate experiments were performed, and the average value was compared to the predicted value.

3.13. Adsorption Isotherms and Kinetic Studies

Isotherms and kinetic models were examined to study the adsorption capacity and rate of adsorption of IBP onto a magnetized SCGB–chitosan composite adsorbent.

3.13.1. Adsorption isotherms

The equilibrium relationship between the amount of IBP adsorbed and the amount remaining in solution has been established using the adsorption equilibrium model. Both the Langmuir and Freundlich isotherm models were examined to fit the experimental data. The equilibrium adsorption capacity of IBP was calculated using the equation (3.6).

$$q_e = \frac{(C_i - C_e) \times V}{m} \quad \text{.....(3.6)}$$

Where q_e is the amount of adsorbate adsorbed at equilibrium (mg/g), c_i, c_e, V and m is the initial concentration of IBP (mg/L), the concentration of IBP at equilibrium (mg/L), and volume of IBP solution (L) and mass of adsorbent (g) respectively (Al-Obaidi et al., 2023).

Langmuir Isotherm Model

Langmuir adsorption isotherm deals with the following assumptions

1. Adsorption is taking place in a monolayer homogenous surface of adsorbent of identical sites that are equally available;

2. Molecules are adsorbed at discrete active sites on the surface and the saturation point will reach;
3. Energetically uniform adsorbent surface;
4. No interaction between adsorbate molecules;

The linear form of Langmuir isotherm is given by: -

$$\frac{C_e}{q_e} = \frac{C_e}{q_m} + \frac{1}{q_m K_1} \quad \text{.....(3.7)}$$

Where the values of the Langmuir rate constant K_1 (L/kg) and maximum adsorption capacity $q_m(\frac{mg}{g})$ are obtained from the slope and intercept of $\frac{1}{q_e}$ vs $\frac{1}{c_e}$ plot respectively and C_e, q_e, stands for the equilibrium concentration of IBP in (mg/l) and mg/g respectively. The maximum theoretical IBP adsorbed and the Longmuir constant related to the affinity of binding (L/mg) respectively (Alqarni et al., 2024).

Freundlich Isotherm Model

The Freundlich isotherm model is derived from the assumption of adsorption taking place on multilayer a heterogeneous adsorption site. It is used to describe non-ideal and reversible adsorption processes. The linear form of Freundlich adsorption isotherm can be formulated as:

$$lnq_e = lnK_f + \frac{1}{n} lnC_e \quad \text{.....(3.8)}$$

Where Ce is the concentration of IBP at equilibrium in the solution, q_e is the amount of IBP adsorbed at equilibrium, and 1/n shows a more heterogeneous surface which implies that as the value of 1/n approaches one, the adsorbent approaches to the more homogenous binding site. Where the value of the inverse of adsorption intensity 1/n and Fruendlich constant k_f are obtained from the slope and intercept of the $\ln(q_{e)}$vs $\ln(c_e)$ graph (Adane et al., 2020).

3.13.2. Kinetic studies

The rate of adsorbate uptake and the mechanism of the adsorption process can be studied using Pseudo first order (PFO), Pseudo second order (PSO), and Intraparticle diffusion (IPD) kinetic models. To investigate the rate of adsorption and the controlling mechanisms, such as mass transfer and chemical reactions, the PFO, PSO, and IPD equations were applied to the model. This analysis focuses on the kinetics of IBP adsorption onto a magnetized SCGB-chitosan composite adsorbent (Wang & Guo, 2020).

To investigate IBP adsorption on a magnetized SCGB-chitosan composite, 0.12 g of adsorbent was added to 60 mL of an IBP solution with an initial concentration of 2.5 mg/L in a 200 mL flask. The solution was stirred at 200 rpm for 30 minutes for homogeneity. Contact times were varied at 20, 40, 60, 80, and 100 minutes to study the adsorption kinetics. At the end of each experiment, the filtrate was analyzed for IBP concentration using a UV-visible spectrophotometer at 222 nm. The amount of IBP adsorbed was calculated using equation 3.9 (Aarab et al., 2020).

$$q_t = \frac{(C_i - C_t) \times V}{m} \quad \text{.....(3.9)}$$

Where q_t (mg/g) is the amount of IBP adsorbed at time t, C_i the initial concentration of IBP (mg/L), C_t (mg/L) the concentration of IBP in the solution at time t, V (L) is the volume of the solution, and m (g) is the adsorbent dosage.

Pseudo First Order (PFO) Kinetic Model

The PFO kinetic model assumes that the rate of adsorbate uptake is directly proportional to the number of available active sites in the adsorbent material. The suitability of this model was evaluated using a linearized formula, as shown in the equation 3.10.

$$\ln(q_e - q_t) = \ln(q_e) - k_1 t \quad \text{.....(3.10)}$$

Where k_1(1/min) is the PFO rate constant and t is the adsorption time (min). The values of k_1 and $q_e$can be determined from the slope and intercept of the linear plot of $\ln(q_e - q_t)$ versus t, respectively.

Pseudo Second Order (PSO) Kinetic Model

The PSO assumes that the adsorption rate is directly proportional to the concentration of IBP. The data used to fit the model are represented using linear as shown in equation below.

$$\frac{t}{q_t} = \frac{1}{q_e^2 k_2} + \frac{1}{q_e} \quad \text{.....(3.11)}$$

Where K_2 ($gmg^{-1}min^{-1}$) is the PSO rate constant. The values of K_2 and q_e can be calculated from the slope and intercept of the $\frac{t}{q_t}$ versus t linear plot (Umejuru et al., 2023)

3.14. Reusability Test

The regeneration experiment was done to determine the economic feasibility of the magnetized SCGB-chitosan-PVA composite adsorbent. The regeneration procedure was initiated through decantation of the adsorbent which was in solution with the help of an external magnetic field. During batch experiments, it was then moistened in 100 mL of ethanol over a period of 2-3 hours and distilled water added so that it could be washed and easy to regenerate. Five adsorption/desorption cycles were carried out and after each cycle, the remaining concentration of IBP was measured (Mojiri et al., 2019).

CHAPTER FOUR

RESULTS AND DISCUSSION

4.1. Yield of Spent Coffee Ground Biochar (SCGB)

The yields of the biochar prepared by different temperatures are consistent with reported values of previous researches which are in the range of 20 and 30% (de Souza et al., 2022). A summary of these yields is presented in Table 4.1 below.

Table 4.1: Production yield of Biochar for various Temperatures

Sample	Experimental Value (Wt.%)
BC500	28.68
BC550	26.72
BC600	24.04

4.2. Characterization of SCGBs and SCGB-Magnetite-Chitosan-PVA Composites

4.2.1. Proximate analysis of SCG

The proximate characterization of SCG, which has low moisture and low ash content as shown in Table 4.2, suggests its potential use as a stable, largely organic material for various valorization routes, including adsorbent development, biochar production, and incorporation in composites. These parameters are crucial for understanding its storage, processing behavior, and performance in applications.

Table 4.2: Proximate Analysis of SCG

Proximate Analysis	Value (Wt%)
Moisture Content,	5.15
Ash Content,	1.36

4.2.2. Surface area analysis of biochars, magnetite, and composites

Based on the specific surface area analysis presented in Table 4.3, the specific surface areas for BC500, BC550, BC600, Magnetite, Composite (75:25), Composite (50:50), and Composite (25:75) are 652.421 m²/g, 469.700 m²/g, 437.750 m²/g, 427.961 m²/g, 524.650 m²/g, 489.250 m²/g, and 463.750 m²/g, respectively. Among the biochars carbonized at different temperatures (BC500, BC550, and BC600), BC500 was selected for composite preparation due to its higher specific surface area. The specific surface area of the composites decreased compared to that of the biochar, likely because the magnetite particles were embedded in the pores of the biochar (Ngernyen et al., 2023). Finally, among the composites prepared at different biochar to chitosan ratios, the Composite (75:25) ratio was chosen for its higher specific surface area for adsorption.

Table 4.3: BET surface area of biochars, magnetite, and composites

Sample	Surface area (m^2/g)
BC500	652.421
BC550	469.700
BC600	437.750
Magnetite	427.961
Composite (75:25)	524.650
Composite (50:50)	489.250
Composite (25:75)	463.750

4.2.3. FTIR analysis of biochars and composites

FTIR analysis was conducted using biochar samples to verify the functional groups present on the material's surface before and after composite preparation. As shown in Figure 4.1 (a), all biochar samples produced at different temperatures exhibited almost similar bands and characteristics typical of carbonaceous materials. The FTIR spectra of the biochar samples revealed bands corresponding to the stretching of aliphatic C–H bonds at 2994 and 2877 cm^{-1}. Bands between 1791 and 1486 cm^{-1} can be attributed to the C=O bond stretch of carboxylic acids and ketones, as well as the stretching of N–H bonds in secondary amines. Additionally, a band at 1411 cm^{-1}, corresponding to the symmetrical stretching of CH_3, was observed. The band around 1228 cm^{-1} is associated with N–H bonds and the stretching of the –OH bond in

carboxylic acids and phenols. A medium-intensity band was observed at 1158 cm^{-1}, corresponding to C–O–C vibrations, indicating the presence of cellulosic components in the sample. The stretching of C–OH vibrations was observed at 1073 cm^{-1}, and finally, a characteristic band of vibrations of C–H groups in aromatic structures appeared at 663 cm^{-1}(Oliveira et al., 2021).

However, the composite's FTIR spectra shows modifications in the functional groups present compared to the biochar. As shown in Figure 4.1 (b), all composite samples produced at different ratios exhibited similar bands and characteristics typical of carbonaceous materials. The bands at 2993 and 2877 cm^{-1} (aliphatic C–H stretch) arise from the $–CH_2–$ groups within PVA as well as aliphatic residues found in the biochar and chitosan (Oliveira et al., 2021). The peak at 1781 cm^{-1} (C=O stretch) indicates a strong carbonyl peak, likely caused by residual ester and acetate groups of PVA (–O–C=O–) from partially hydrolyzed PVA, as well as N-acetyl or amide residues in chitosan. This band is slightly higher than the amide-I band (1650 cm^{-1}), indicating that the ester and acetate groups of PVA dominate this band. Coordination of Fe^{3+} with C=O can also cause this band to shift (Eivazzadeh-Keihan et al., 2023). The range 1600–1500 cm^{-1} contains a mixture of C=C vibrations from biochar and CH_2 vibrations from PVA and chitosan (Lessa et al., 2018). The band at 1580–1610 cm^{-1} is attributed to the aromatic skeleton of biochar. The bands at 1392 & 1317 cm^{-1} are due to CH bending in PVA and chitosan, as well as amide-III and C–N vibrations in chitosan at 1315–1325 cm^{-1} (de Souza et al., 2022). The intensities of these bands confirm the presence of chitosan. The bands at 1180 cm^{-1} and 1041 cm^{-1} (C–O/C–O–C) stretches are strong markers for C–O of PVA, C–O–C of the pyranose ring of chitosan, and phenolic or ether C–O of biochar (Song et al., 2020). The intense band at 1142–1085 cm^{-1} is characteristic of crystallinity in PVA; shifts or broadening may indicate hydrogen bonding with chitosan or biochar, or coordination to Fe–O sites. The peak at 816 cm^{-1} represents aromatic C–H vibrations of biochar as well as ring modes of chitosan (Oliveira et al., 2021). The range 560 cm^{-1} sloping downward towards 480 cm^{-1} indicates the Fe–O stretching of magnetite (Fe_3O_4) (Kassahun et al., 2025).

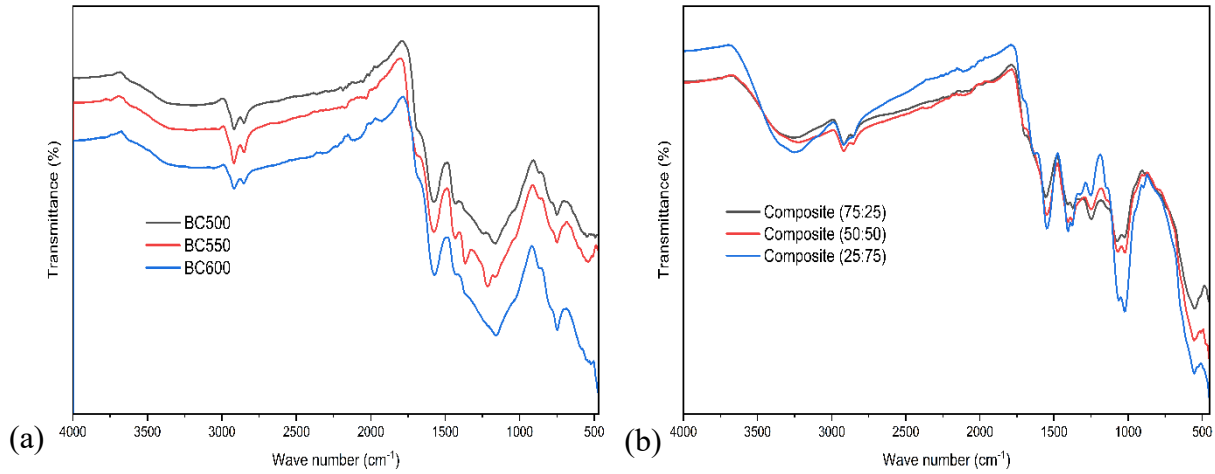

Figure 4.1: FTIR spectra of (a) Biochars and (b) Composite

4.2.4. XRD analysis

XRD analysis was used to evaluate the degree to which the samples were crystalline or amorphous. When a substance is crystalline, well-defined peaks can be observed, whereas non-crystalline or amorphous materials exhibit broad peaks (Ngernyen et al., 2023). The XRD data of the composite (75:25), as shown in Figure 4.2, consists of magnetite, SCGB, chitosan, and PVA. The highest peaks for diffraction are found at 2θ = 11°, 26.5°, 27°, 36°, 48.8° and 49.4°, typical of magnetite in the pattern. The exposed angles correspond to the (220), (311), (400), (422), (440), and (511) planes of the cubic spinel structure of magnetite, as confirmed by JCPDS card no. 85-1436 (Gutierrez et al., 2024). Such sharp outlines indicate that the magnetite in the composite is still highly crystallized and pure, significantly influencing the XRD profile. In contrast, the amorphous structure of SCGB, the semi-crystalline structure of chitosan, and PVA contribute to the cloudy background and low intensity in the range of 12-25° and 51-60^{o} (Changotra et al., 2023; Kaur et al., 2024). The lack of sharply changing peaks or numerous stages suggests that the dispersion and relationship between the composite elements are efficient, with no significant alterations to the elements. Consequently, based on the XRD pattern, this is a composite where magnetite crystallites dominate the crystallinity, while the amorphous matrix consists of a blend of biochar, chitosan, and PVA, enhancing the multifunctional application of each component and providing synergistic properties.

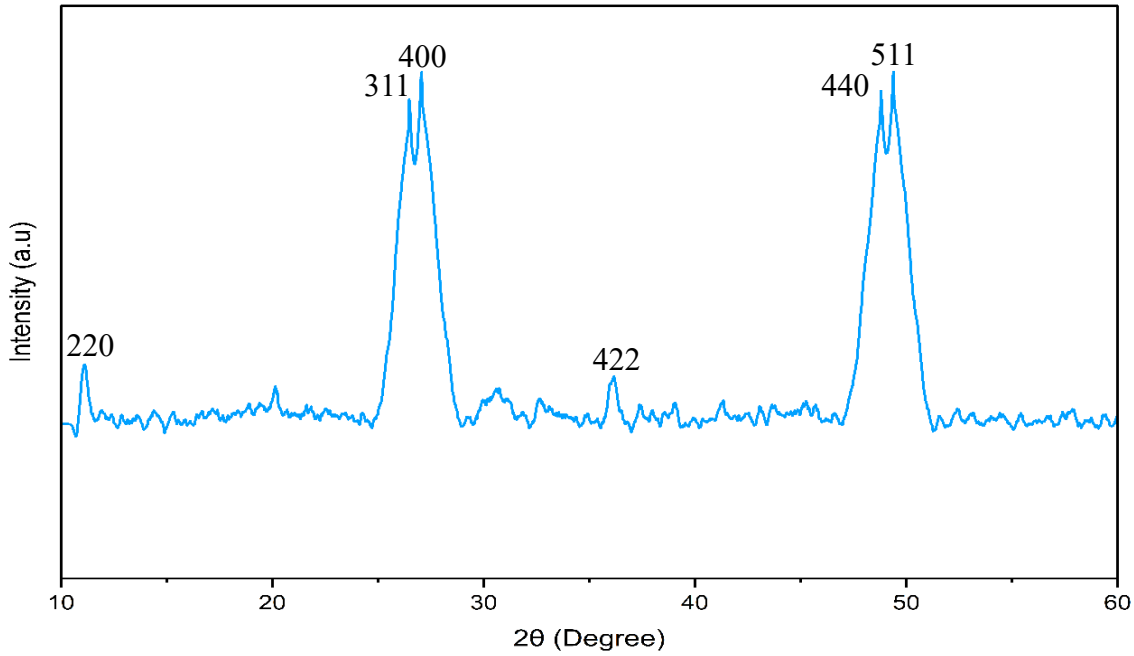

Figure 4.2: XRD pattern of composite (75:25)

4.2.5. Scanning electron microscope (SEM) analysis

Figure 4.3 demonstrates the SEM images of the surface morphology of Composite (75:25). At the lower optical magnification of 500X as shown in figure 4.3 (a), the structure of the porous and agglomerated powder is observed to be comprised of huge, massive clusters of particles with huge empty spaces in between of a wide range of sizes. On further magnification of the figure 4.3 (b) with 1000X magnification, the individual morphology of the primary particles can be observed, as indicated by the flaky particles with a wide size distribution and the high level of agglomeration. Figure 4.3 (c) of 3000X reveals a more or less the same construction with a high density of spongy fine pore network in relation with big agglomerated particles. Lastly, the largest magnification resulting in best resolution is figure 4.3 (d) of 10,000X magnification depicting a lot of agglomeration and high porosity. All these SEM images prove that Composite (75:25) can be used in adsorbing.

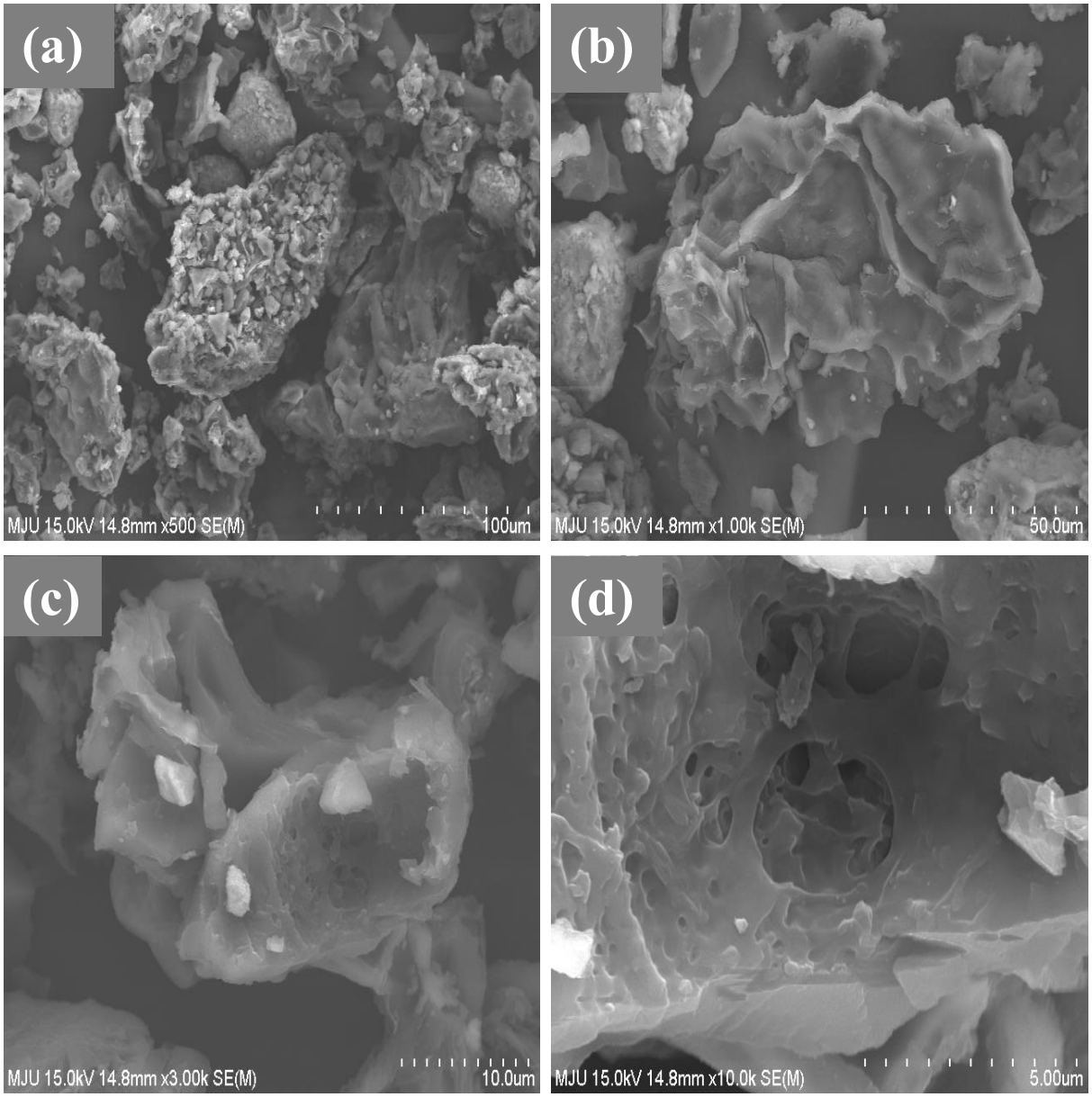

Figure 4.3: SEM images of Composite (75:25) at resolutions of (a) 500, (b) 1k, (c) 3k, and (d) 10k

4.2.6. Energy dispersive X-ray spectroscopy (EDX) analysis

Energy Dispersive X-ray Spectroscopy **(**EDX) was performed to fully describe the elemental composition of the material. The outcomes include a spectrum of the results and a quantitative analysis. The table presents the atomic and weight percentages of the detected elements, while figure 4.4 shows the EDX spectrum with the characteristic X-ray emission peaks. The biochemical structure is primarily composed of iron (Fe) at 53.66 percent and oxygen (O) at 34.56 percent, indicating that the main chemically distinct component is magnetite (Fe_3O_4). The deviation between the stoichiometric percentages of pure magnetite (72.4% Fe, 27.6% O)

suggests the inclusion of an oxygen-rich organic skeleton, along with a high concentration of carbon (C) at 10.04%, which is attributed to the SCGB, chitosan, and PVA polymers. The discovery of minor and trace elements is consistent with the anticipated composition and synthesis pathway. The presence of chlorine (Cl) at 1.65% is likely due to iron chloride precursors used in the magnetite synthesis, while small traces of calcium (Ca) at 0.09% and potassium (K) at 0.01% are typical of the mineral constituents of the exhausted SCGB. In summary, the EDX spectrum indicates the effective incorporation of all constituents, and the elemental profile reflects the inorganic magnetite filler and the organic matrix, along with some traces of process-related residues.

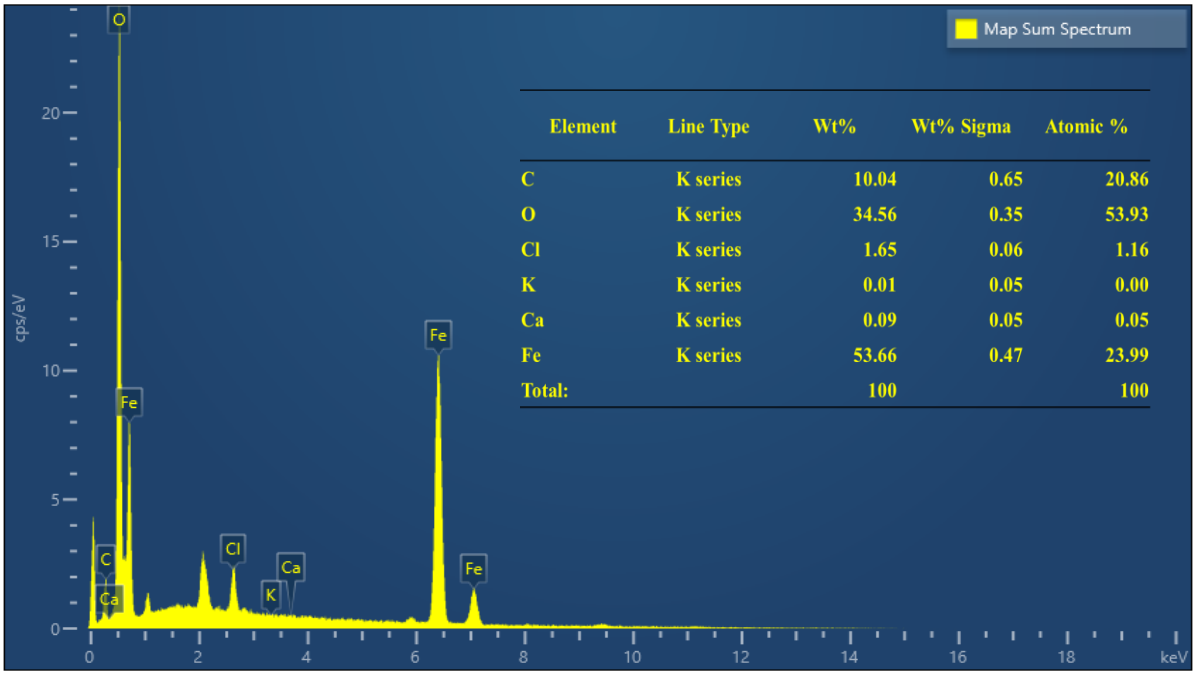

Element	Line Type	Wt%	Wt% Sigma	Atomic %
C	K series	10.04	0.65	20.86
O	K series	34.56	0.35	53.93
Cl	K series	1.65	0.06	1.16
K	K series	0.01	0.05	0.00
Ca	K series	0.09	0.05	0.05
Fe	K series	53.66	0.47	23.99
Total:		100		100

Figure 4.4: EDX elemental analysis of composite (75:25)

4.3. Experimental Runs based on Central Composite Design (CCD)

Table 4.4 shows the experimental runs of the Central Composite Design (CCD). The four parameters analyzed were the dosage of composite adsorbent, contact time, initial pH of the solution, and initial IBP concentration. The table includes the measured (laboratory) values of the IBP removal percentage at different adsorption parameters.

Table 4.4: CCD Experimental runs with factor levels and response data

Order	Factors				Response
Run	pH	Conc.(mg/L)	Dosage (g/L)	Time (min)	IBP Removal Efficiency (%)
					Actual Value
1	4	5.0	2.0	80	96.07
2	4	10.0	2.0	40	71.58
3	4	5.0	1.0	80	86.59
4	6	2.5	1.5	60	95.12
5	8	10.0	1.0	40	39.55
6	6	12.5	1.5	60	74.74
7	6	7.5	1.5	60	76.21
8	6	7.5	0.5	60	64.21
9	6	7.5	2.5	60	94.79
10	4	10.0	1.0	80	80.55
11	4	10.0	1.0	40	58.49
12	8	5.0	1.0	40	54.96
13	6	7.5	1.5	60	75.91
14	6	7.5	1.5	20	48.98
15	10	7.5	1.5	60	34.67
16	4	5.0	1.0	40	66.13
17	8	5.0	2.0	40	64.43
18	8	10.0	2.0	40	53.75
19	4	5.0	2.0	40	76.90
20	8	5.0	1.0	80	73.87
21	6	7.5	1.5	100	93.89
22	8	10.0	2.0	80	78.19
23	6	7.5	1.5	60	74.96
24	4	10.0	2.0	80	92.89
25	2	7.5	1.5	60	61.48
26	6	7.5	1.5	60	74.48
27	8	10.0	1.0	80	56.94
28	6	7.5	1.5	60	74.59
29	6	7.5	1.5	60	77.01
30	8	5.0	2.0	80	85.45

4.4. Statistical Analysis for IBP Removal

4.4.1. Sequential model sum of squares

The IBP removal efficiency was evaluated using the Sequential Model sum of Squares (Type I). The straight-line term explained much of the variation in response and was highly significant ($p < 0.0001$). Adding two-factor interaction (2FI) terms after the linear term did not provide a significant value ($p = 0.9872$). However, the inclusion of a quadratic term significantly improved the model fit ($p < 0.0001$, F-value = 158.64), indicating a strong non-linear relationship. A cubic term was tested but was not statistically significant ($p = 0.0370$) and was identified as "Aliased," indicating it could not be used in this model. Thus, the quadratic model was selected as the best representation of IBP removal efficiency.

Table 4.5: Sequential model sum of squares

Source	Sum of Squares	Df	Mean Square	F-value	p-value	
Mean vs Total	1.55E+05	1	1.55E+05			
Linear vs Mean	5679.42	4	1419.86	19.71	< 0.0001	
2FI vs Linear	80.57	6	13.43	0.1483	0.9872	
Quadratic vs 2FI	**1680.64**	**4**	**420.16**	**158.64**	**< 0.0001**	**Suggested**
Cubic vs Quadratic	32.89	8	4.11	4.21	0.037	Aliased
Residual	6.84	7	0.9772			
Total	1.63E+05	30	5424.62			

4.4.2. Analysis of variance (ANOVA)

The Model F-value of 200.66 indicates that the model is significant, with only a 0.01% chance that an F-value this large could occur due to random noise. P-values less than 0.0500 demonstrate that the model terms are significant. In this case, the significant model terms are A, B, C, D, AB, BC, A^2, B^2, C^2, and D^2. Conversely, values greater than 0.1000 suggest that the model terms are not significant. If there are many insignificant model terms (excluding those necessary to support hierarchy), reducing the model may improve its performance. The Lack of Fit F-value of 3.39 indicates a 9.52% chance that a Lack of Fit F-value this large could

arise from random noise. Lack of fit is undesirable; we want the model to fit well. This relatively low probability (<10%) is concerning.

Overall, this ANOVA suggests that the quadratic model is a robust and suitable fit for the IBP removal efficiency data, clearly highlighting the significant main and curvilinear effects of the experimental parameters studied. Table 4.6 presents the ANOVA results for the selected quadratic model.

Table 4.6: ANOVA for the quadratic model fitted to the experimental data

Source	**Sum of Squares**	**Df**	**Mean Square**	**F-value**	**p-value**	
Model	**7440.64**	**14**	**531.47**	**200.66**	**< 0.0001**	**Significant**
A-pH	1297.64	1	1297.64	489.94	< 0.0001	
B-conc	541.72	1	541.72	204.53	< 0.0001	
C-dosage	1122.63	1	1122.63	423.86	< 0.0001	
D-time	2717.42	1	2717.42	1025.99	< 0.0001	
AB	46.6	1	46.6	17.6	0.0008	
AC	6.27	1	6.27	2.37	0.1446	
AD	0.26	1	0.26	0.0981	0.7584	
BC	22.04	1	22.04	8.32	0.0113	
BD	1.46	1	1.46	0.5527	0.4687	
CD	3.92	1	3.92	1.48	0.2423	
A^2	1286.49	1	1286.49	485.73	< 0.0001	
B^2	153.45	1	153.45	57.94	< 0.0001	
C^2	27.85	1	27.85	10.52	0.0055	
D^2	27.91	1	27.91	10.54	0.0054	
Residual	39.73	15	2.65			
Lack of Fit	**34.62**	**10**	**3.46**	**3.39**	**0.0952**	**not significant**
Pure Error	5.11	5	1.02			
Cor Total	7480.36	29				

4.4.3. Fit statistics

Fit statistics were used to evaluate the overall quality and reliability of the model. The observed high R^2 value of 0.9947 indicates that approximately 99.5% of the variation in IBP removal efficiency can be explained by the model. This strong explanatory power is further supported by an Adjusted R^2 of 0.9897, which accounts for the number of terms in the model and remains very high. Additionally, the model demonstrated predictive power with a predicted R^2 value of 0.9724. The predicted R^2 shows reasonable agreement with the Adjusted R^2, as their difference is less than 0.2, which is generally regarded as a positive indicator of model robustness.

The Adequate Precision, an important measure of the signal-to-noise ratio and model quality, was 55.6269, significantly exceeding the acceptable ratio of 4. This indicates that a satisfactory signal can be obtained, validating the model's suitability for exploring the design space. Other measures, such as a standard deviation of 1.63 and a coefficient of variation (C.V. %) of 2.26, were also noted. Together, these fit statistics provide strong evidence of an excellent model fit, good predictive capability, and overall reliability in representing the IBP removal efficiency data.

Table 4.7: Fit summary for the developed model

Std. Dev.	1.63	R^2	0.9947
Mean	71.94	Adjusted R^2	0.9897
C.V. %	2.26	Predicted R^2	0.9724
		Adeq Precision	55.6269

4.4.4. Diagnostic plots

To assess the accuracy of the developed model, two diagnostic plots corresponding to the most important regression assumptions were selected. These plots are used to evaluate the model assumptions, assess the adequacy of the model, examine the independence and randomness of experimental errors, review the residuals for each independent factor, and determine the model's performance. The plots effectively demonstrate the model’s reliability.

4.4.4.1. Normal probability plot of residuals

A normal plot of residuals was created to assess the model's assumptions. This plot provides a visual examination of whether the residuals (i.e., the differences between observed and predicted values) are normally distributed. The best fit for the data points is a straight line that diagonally crosses the plot. A perfect line indicates that the model's residuals are normally distributed, which is a fundamental assumption for many statistical tests, including ANOVA. From the plot in Figure 4.5, the data points were observed to be relatively close to the straight line, suggesting that the residuals are normally distributed. This visual fit validates the model formulation and the subsequent analyses conducted with the model.

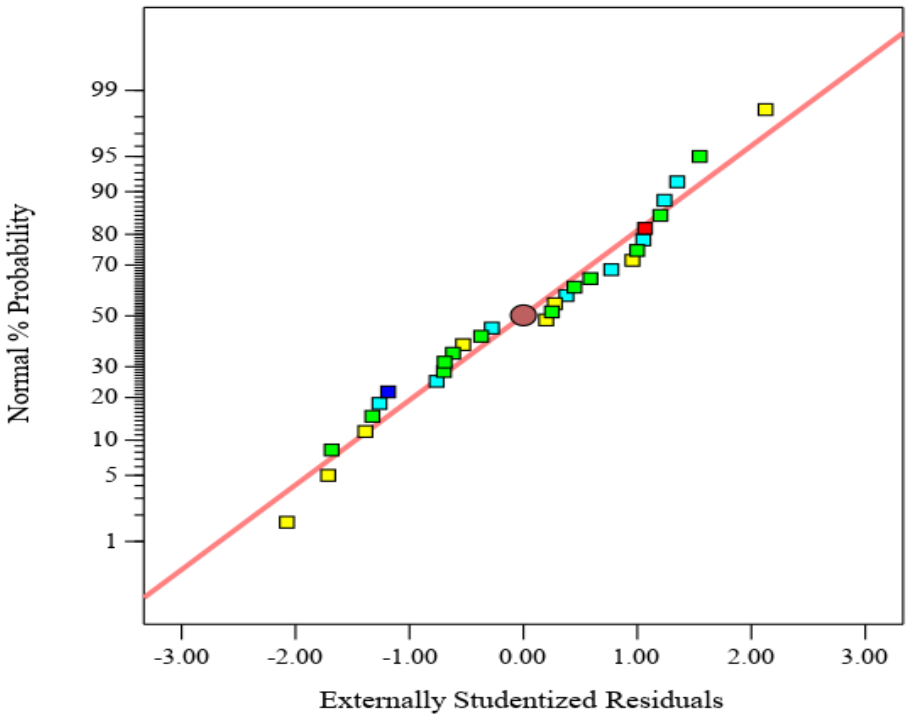

Figure 4.5: Normal plot of Residuals for IBP removal efficiency

4.4.4.2. Predicted values Vs actual values plot

The performance of the model was assessed visually using the Predicted versus Actual plot shown in figure 4.6. This plot provides a clear way to demonstrate how closely the model's predictions aligned with the observed results from the experiments. Ideally, if the model were perfect, all data points would lie on the 45-degree line, indicating that predicted values equal actual values. In the plot resulting from this study, most data points were close to this ideal

straight-line relationship. The predicted values closely matched the actual IBP Removal Efficiency measured during the experiments. The scatter of data points around the dashed line appeared consistent, further confirming the model's reliability across the range of IBP removal efficiencies. Overall, the evidence was promising, indicating a developed model with strong predictive capabilities and a reliable estimation of IBP Removal Efficiency under the conditions of this study.

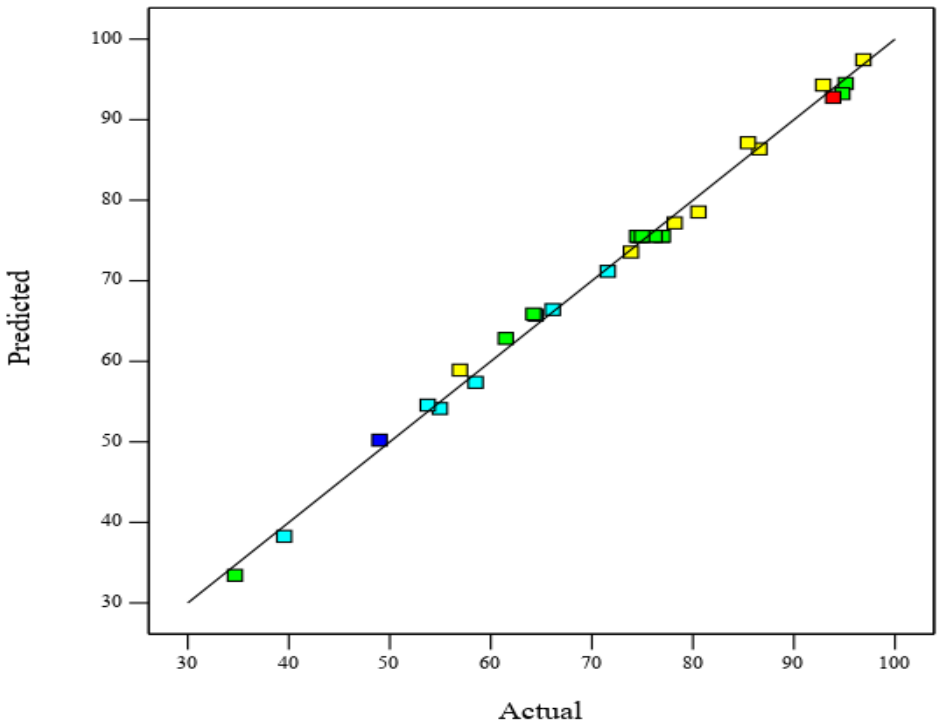

Figure 4.6: Actual vs predicted values for IBP removal efficiency

4.4.5. Combined effects of the independent variables

Figures 4.7 (a), (b), (c), (d), (e), and (f) illustrate the interaction effects of the process variables contact time, initial pH of the solution, initial concentration of IBP, and adsorbent dosage on removal efficiency, while keeping the other operational variables constant.

Figure 4.7 (a) depicts the interaction effect of the initial IBP concentration and solution pH across all contact times and adsorbent dosages. As shown in the figure, removal efficiency decreases as the pH rises from 6 to 10 and as the initial IBP concentration increases from 2.5 mg/L to 12.5 mg/L due to the limited active sites available on the adsorbent's surface at a given dosage. The highest removal efficiency was achieved at an initial concentration of 5 mg/L and

a solution pH of around 4. This may be attributed to the more positively charged adsorbent surface at this pH, which enhances the electrostatic attraction of IBP molecules. Conversely, the lowest removal efficiency was observed at higher pH levels, except under neutral conditions, along with varying adsorbent dosages and higher initial IBP concentrations.

Similarly, figure 4.7 (b) illustrates the combined effect of initial solution pH and adsorbent dosage. Removal efficiency increases as the adsorbent dosage rises from 0.5 g/L to 2.5 g/L and as the pH increases from 2 to 6 at a given adsorbent dosage. The maximum removal efficiency occurs at an acidic pH and a higher adsorbent dosage. This finding indicates that solution pH negatively affects and adsorbent dosage positively impacts the removal efficiency, supporting previous research.

Figure 4.7 (c) illustrates the interaction effect between initial solution pH and contact time. Removal efficiency improves as contact time increases from 20 to 100 minutes and as the initial solution pH rises from 2 to 6, while it decreases as pH increases from 6 to 10. According to the model equation, the combined effect of initial solution pH and contact time has a negative impact on removal efficiency, as indicated by a coefficient of -0.0032.

Figure 4.7 (d) illustrates the combined influence of the initial concentration of IBP and adsorbent dosage on IBP removal efficiency. It was found that increasing the adsorbent dosage from 0.5 to 2.5 g/L, while decreasing the initial concentration of IBP from 12.5 to 2.5 mg/L, enhances removal efficiency. The interaction effect of adsorbent dosage and initial IBP concentration has a positive impact on removal effectiveness, as indicated by the model equation. The maximum removal efficiency of IBP is observed at higher doses and lower initial concentrations.

Figure 4.7 (e) depicts the combined effect of contact time and initial concentration of IBP within a specified range of solution pH and adsorbent dosage. The removal of IBP increases as the contact duration extends from 20 to 100 minutes and the initial concentration decreases from 12.5 to 2.5 mg/L, as illustrated by the 3D plot. This increase is attributed to the extended contact time, which allows IBP molecules ample opportunity to interact with the adsorbent surface, leading to higher removal efficiency. Conversely, the removal of IBP decreases as the initial concentration increases from 2.5 to 12.5 mg/L due to the limited availability of active sites on the adsorbent surface at a dosage of 2 g/L. The interaction effect of contact time and

initial concentration of IBP positively impacts removal efficiency, as indicated by the model equation.

Figure 4.7 (f) illustrates the interaction effect between contact time and adsorbent dosage on removal efficiency. As contact time increases from 20 to 100 minutes and adsorbent dosage rises from 0.5 g/L to 2.5 g/L while maintaining a constant pH and an initial IBP concentration of 5 mg/L, the removal efficiency also improves. This interaction effect positively influences removal effectiveness, with a coefficient of +0.05. The increase in removal efficiency can be attributed to a higher adsorbent dosage, which provides more available sites for the adsorption of IBP. The maximum removal efficiency of 96.07% was achieved at 80 minutes of contact time with a 2 g/L adsorbent dosage.

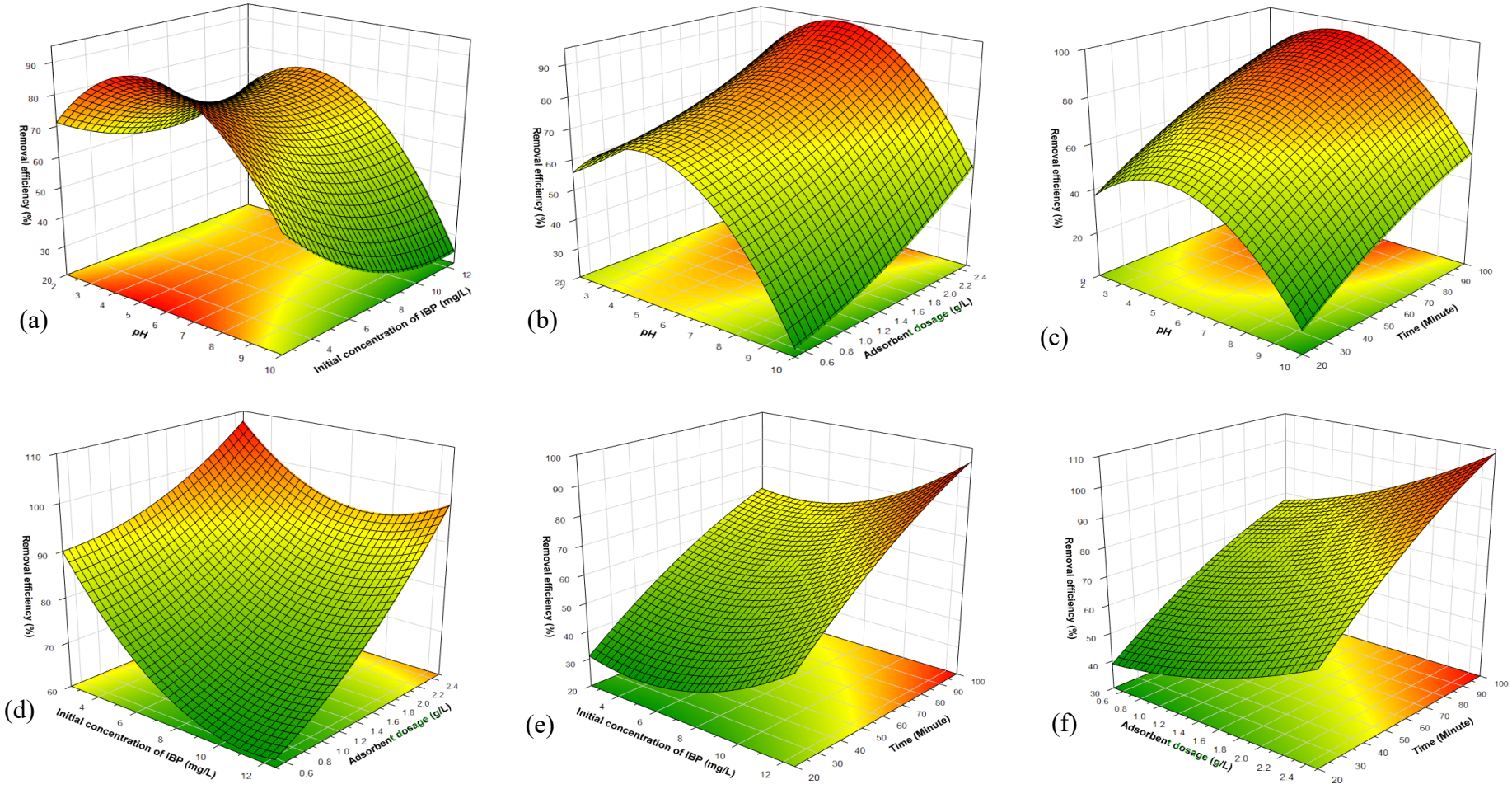

Figure 4.7: Interaction effect of (a) pH Vs initial concentration of IBP, (b) pH Vs adsorbent dosage, (c) pH Vs time, (d) Initial concentration Vs adsorbent dosage, (e) Initial concentration Vs time, and (f) adsorbent dosage Vs time

4.5. Statistical Optimization of Process Variables

After studying the interaction effects of operating parameters, a statistical optimization was conducted to determine the conditions for optimum adsorption of IBP onto composite (75:25) adsorbent. The interaction effects of the operating parameters on the removal efficiency of the adsorbent material increase with longer contact times and higher adsorbent dosages at a solution pH around 4, while they decrease with rising initial concentrations of IBP. Therefore, these fluctuations must be optimized to achieve the best removal efficiency under ideal operating conditions. The optimum process conditions were selected based on the high removal efficiency values derived from the model equations. Accordingly, Table 4 presents the optimization constraints and maximizes the response.

Table 4.8: Optimization constraints on operational factors and response.

Name	Goal	Lower Limit	Upper Limit
A: pH of the solution	is in range	4.00	8.00
B: Initial concentration of IBP	is in range	5.00	10.00
C: Adsorbent dosage	is in range	1.00	2.00
D: Contact time	is in range	40.00	80.00
Removal efficiency	maximize	34.67	96.07

As a result, an initial concentration of 5.0 mg/L, a pH of 4.5, a contact time of 80 minutes, and an adsorbent dosage of 2.0 g/L were chosen to achieve a maximum IBP (IBP) removal rate of 96.7%. An experiment was conducted to test the optimal results predicted by the model under these conditions identified through numerical optimization. The actual removal efficiency obtained from the experiment closely matched the expected value (96.12%), demonstrating a variance of less than 1%.

4.6. Adsorption Isotherm and Kinetic Studies

4.6.1. Adsorption isotherms

Adsorption isotherm models provide insights into the adsorption mechanism and are developed to determine the interaction between liquid-phase adsorbate concentrations and solid-phase adsorption amounts. These models correlate theoretical equations with the adsorption process

(Kassahun et al., 2021). In the present study, two well-known isotherm models, namely Freundlich and Langmuir, were investigated under optimized synthesis parameters to determine the adsorption characteristics of the prepared composite adsorbent. The isotherm constant parameters for these models were derived from their corresponding linearized equations:

$$\frac{C_e}{q_e} = \frac{1}{q_{mK_L}} + \frac{C_e}{q_m} \quad \text{.....(4.1)}$$

$$\ln q_e = \ln K_F + \frac{1}{n}\ln C_e \quad \text{.....(4.2)}$$

where Ce is the contaminant equilibrium concentration (mg/L), q_e is the equilibrium amount of contaminant adsorbed (mg/g), and K_L and K_F are the Langmuir and Freundlich constants (L/mg), respectively. q_m represents the maximum adsorbed quantity, and n is the Freundlich adsorption intensity constant. The values of K_L, K_F, q_m, and n were determined from the slopes and intercepts of the two equations after plotting C_e/q_e versus C_e and ln C_e versus ln q_e (Fig. 4.8 a and b). As shown in Table 4.9, the Langmuir isotherm model fits the experimental data better, as indicated by the higher correlation coefficient (R^2 = 0.991). This model typically describes the formation of a monolayer adsorption process on the surface of the adsorbent.

Table 4.9: Isotherm model parameters for IBP adsorption onto Magnetized SCGB-Chitosan composite

Isotherm Models	Constant Parameters				Correlation Coefficient
	q_m	K_L	K_F	n	R^2
Langmuir	1.27	9.44			0.991
Freundlich			1.7	4.7	0.933

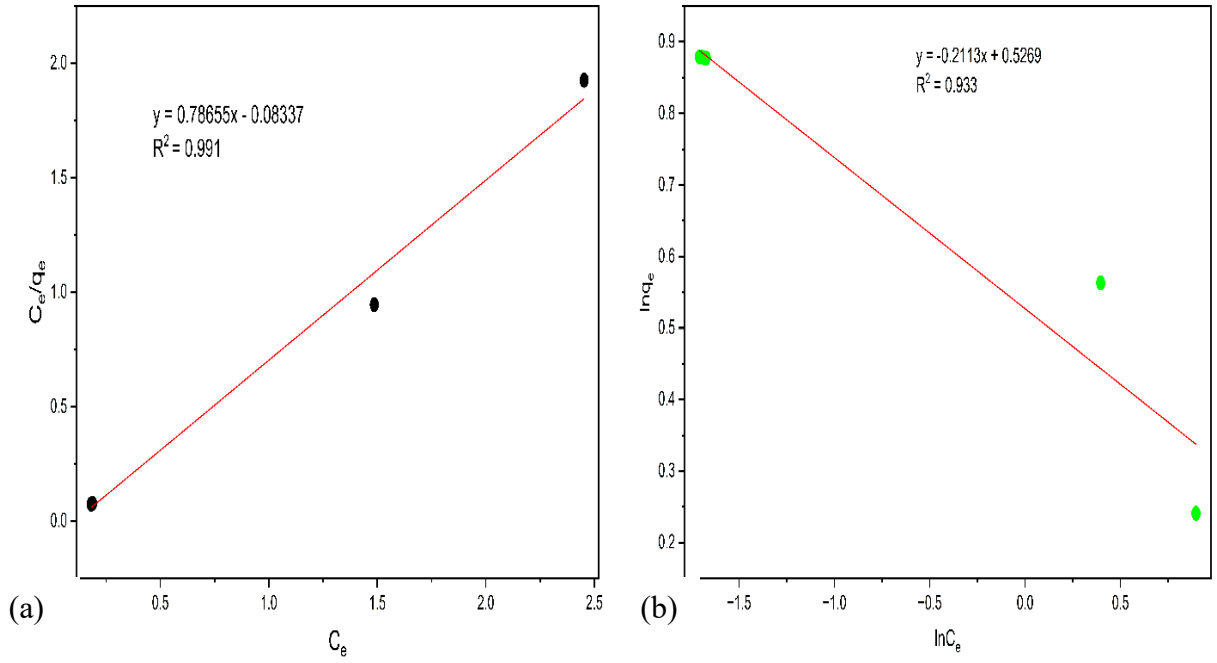

Figure 4.8: Adsorption Isotherm models of (a) Langmuir and (b) Freundlich.

4.6.2. Adsorption kinetic study

The reaction kinetics were investigated to determine the adsorption mechanism. PFO, PSO, and IPD kinetic models were employed in the kinetics study, as represented by the following equations:

$$\text{Log}(q_e - q_t) = \log q_e - \frac{K_1}{2.303} t \quad \text{..... (4.3)}$$

$$\frac{T}{q_t} = \frac{1}{K_2 q_e^2} + \frac{t}{q_e} \quad \text{..... (4.4)}$$

$$q_e = K_i t^2 + C_i \quad \text{..... (4.5)}$$

where, q_e is IBP adsorption amount at equilibrium, q_t is the adsorption amount at any time t, K_1, K_2, and K_i are the rate constants for PFO, PSO, and IPD kinetic models. C_i IPD boundary layer thickness.

Table 4.10: Pseudo first order, pseudo second order, and IPD kinetic models' parameters.

Kinetics Model	Parameter	IBP Concentration (mg/L)				
		2.5	**5**	**7.5**	**10**	**12.5**
	K_1	0.0493	0.0436	0.0436	0.0359	0.0401
	$q_{e\ cal}$	1.334	2.758	4.312	6.124	6.901
	$q_{e\ exp}$	1.215	2.41	3.548	4.739	5.414
Pseudo first order	R^2	0.989	0.980	0.986	0.986	0.979
	K_2	0.00658	0.0203	0.0092	0.0048	0.0046
	$q_{e\ cal}$	1.131	2.332	3.629	4.827	5.604
	$q_{e\ exp}$	1.215	2.41	3.548	4.739	5.414
Pseudo second order	R^2	0.998	0.995	0.995	0.993	0.986
	K_i	0.158	0.312	0.463	0.61	0.702
	C_i	0.05	0.026	0.053	0.187	0.175
IPD	R^2	0.883	0.912	0.919	0.930	0.925

For the PFO model equation, the constant K_1 was determined from the straight-line plot of t versus log ($q_e - q_t$) (Fig. 4.9 a). For the PSO model, the value of K_2 was obtained from the plot of t versus t/q_t (Fig. 4.9 b). The IPD kinetic parameter was determined from the plot of $t^{0.5}$ versus q_e (Fig. 4.9 c). The correlation coefficient R^2 values were used to select the best reaction kinetic model. Kinetic parameters for the selected models are presented in Table 4.10 indicates, the PSO kinetic model best describes the reaction process of IBP adsorption on the adsorbent surface. With this model, the calculated IBP removal amount at equilibrium (q_e) closely matched the IBP removal amount at any given time (q_t). According to the PSO kinetic model, the controlling stage appears to be the chemical reaction.

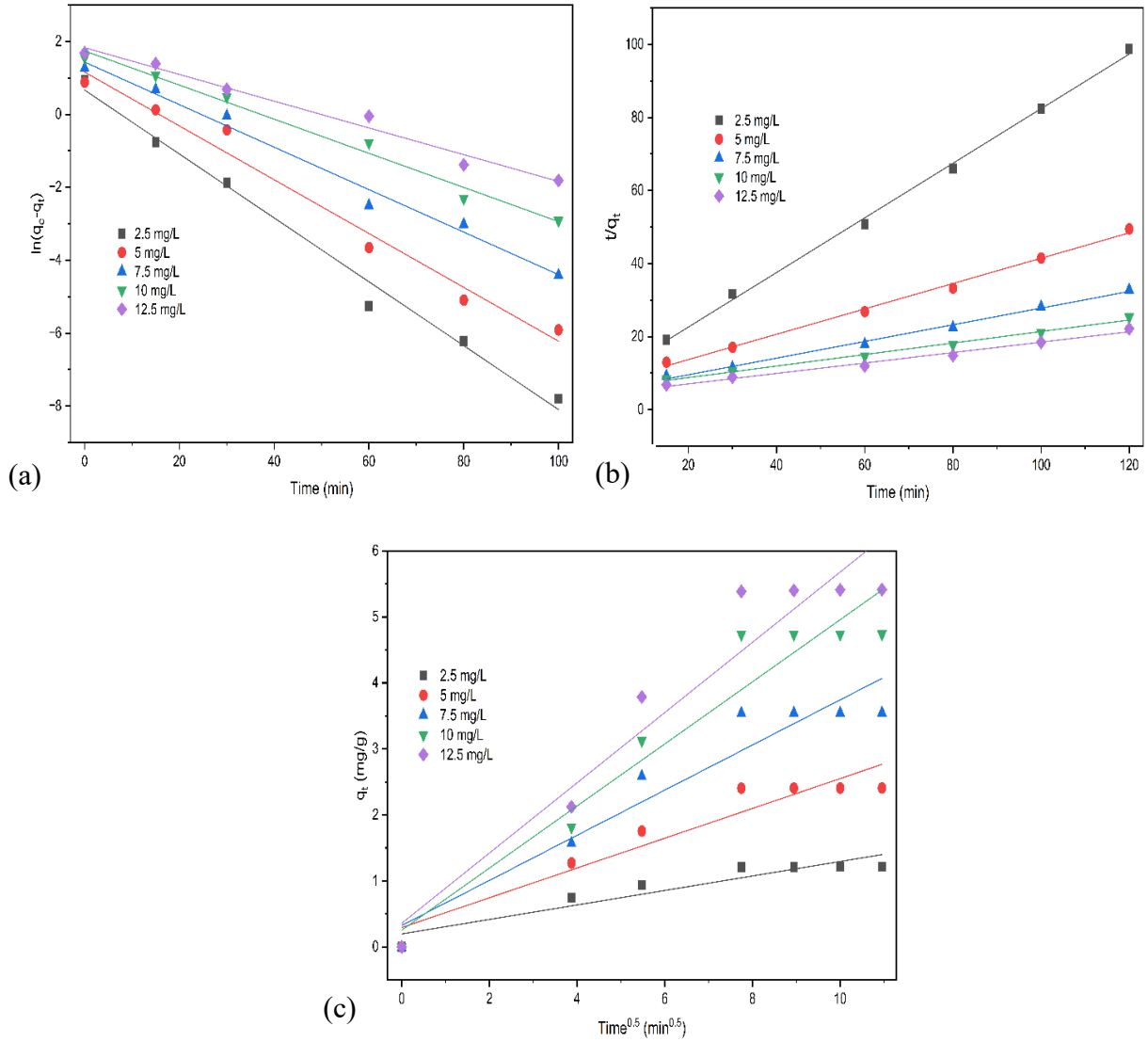

Figure 4.9: Reaction kinetics models of (a) PFO, (b) PSO and (c) IPD.

4.7. Reusability

The process of regenerating adsorbents is a crucial process in wastewater treatment since it incurs less processing expenses. Other regeneration techniques have been used in desorption studies and they include thermal and chemical regeneration. The right choice of pH and desorbents, including inorganic or organic ones, such as ethanol, methanol, and acetic acid, are important when carrying out the chemical desorption process (Mojiri et al., 2019).

The reusability of composite in this study was studied under the optimum operating conditions as per the optimization data. The tests were performed using the initial IBP concentration of 5

mg/L, a dosage of 2.0 g/L adsorbent, and an initial solution pH of 4.5 and 80 min. The appearance of micropollutants may be primarily soluble in alcohols because of the existence of hydroxyl groups, and low molecular weight alcohols can potentially be especially beneficial in terms of the desorption of micropollutants.

The removal efficiency of the adsorbent was mostly constant after four cycles (Figure 4.10) and the removal efficiencies of the four initial cycles were 96.7, 95.3, 93.5, and 88.55, respectively. It was however, in the fifth cycle where the removal efficiency was more pronounced because it dropped to 78.65 percent as compared to 88.55 percent. This loss can be credited to various factors such as loss of stability, leaching and depletion of active sites. Hence, the composite (75:25), which is easy to separate and eco-friendly, has the potential to be a sustainable adsorbent in the removal of IBP in wastewater.

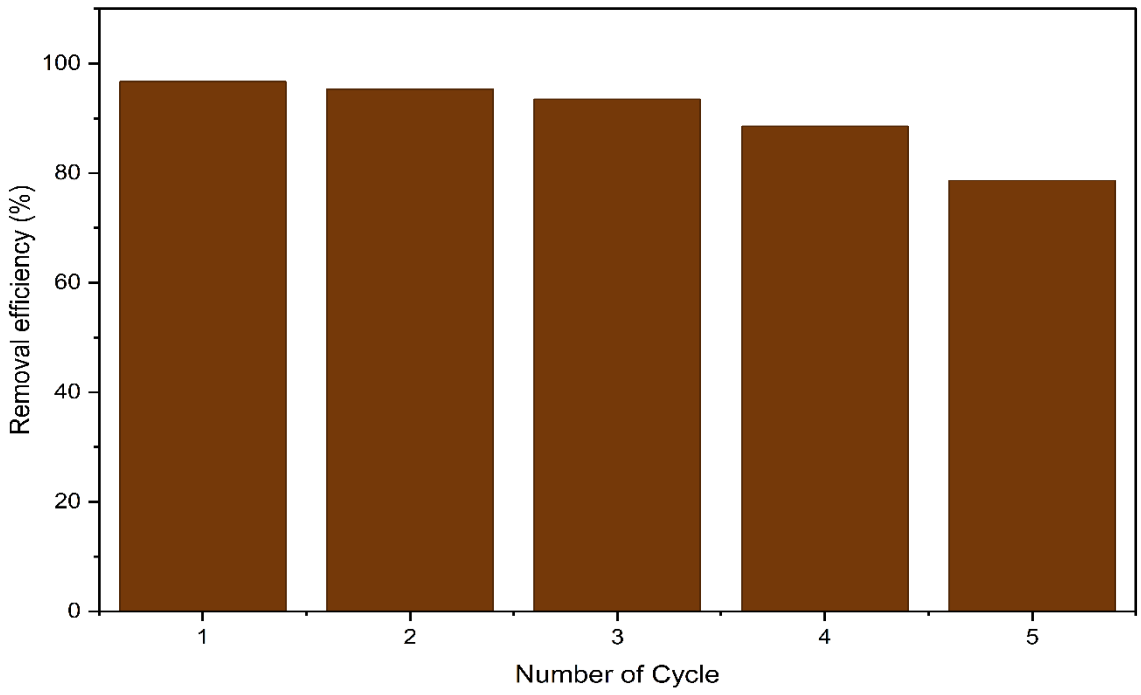

Figure 4.10: The reusability of the composite adsorbent (75:25)

CHAPTER FIVE

CONCLUSIONS AND RECOMMENDATIONS

5.1. Conclusions

A magnetized composite of SCGB and chitosan was prepared with mixing ratios of 75:25 (SCGB to Chitosan), which was used in adsorption experiments. The composite had great adsorptive properties as evidenced by BET, FTIR, SEM, and XRD. The four factors were determined and the effects of their interaction compared and optimized statistically with the help of CCD. It was found that an initial concentration of 5 mg/L, a pH of 4.5, a contact time of 80 minutes, and a dose of adsorbent of 2.0 g/L is optimum to produce the highest IBP removal of 96.7 percent. These methods availed in-depth understanding of the predictive ability of the operational parameters enabling the exploration and optimization of the conditions outside the original range to achieve maximum removal efficiency. The results indicate that statistical experimental design can focus on the exploration of complex processes, including adsorption, when several factors interact concurrently to characterize the performance.

The prepared adsorbent usability was tested in five cycles showing an efficiency of 78.65% in the fifth cycle. Considering this, with the high availability of agricultural waste, SCGB, and its composite have high adsorption efficiency with limited loss experienced after repeated use. The material has some potential to be commercialized on the condition that the technical, economical, and environmental viability of this material is carefully evaluated and assessed when used in pilot-scale as well as large-scale use.

5.2. Recommendations

This paper involved the preparation of a magnetized SCGB-chitosan composite and its use in the removal of IBP in synthetic wastewater during batch trials. To inform future research and make the implementation of such findings practical, the following are the recommendations.

To begin with, the biomass was carbonized in a furnace in the availability of oxygen. It was unrealistic to attain a totally oxygen-free condition despite the fact that the crucibles were sealed with aluminum foil. All experiments should therefore be carried out in furnaces with well controlled inert atmosphere.

Secondly, to further authenticate the sustainability of the suggested approach, new researches ought to include EIA and LCA. The evaluation of these should be based on the use of resources, emissions, and environmental trade-offs of large-scale production.

Third, the scale of this study was that of a laboratory and it did not consider the economic viability of scale up. Therefore, pilot or industrial scale experiments are required to determine cost-effectiveness, challenges in operation, and practicality of continuous systems.

Moreover, the adsorption of IBP was performed in synthetic water and the synthetic wastewater containing other pollutants was not used; these may encompass diverse dyes and heavy metals, which may affect the adsorption process. A more realistic and effective investigation should be done with actual pharmaceutical effluent which contains IBP.

REFERENCES

Aarab, N., Hsini, A., Essekri, A., Laabd, M., Lakhmiri, R., & Albourine, A. (2020). Removal of an emerging pharmaceutical pollutant (metronidazole) using PPY-PANi copolymer: Kinetics, equilibrium and DFT identification of adsorption mechanism. Groundwater for Sustainable Development, 11. https://doi.org/10.1016/j.gsd.2020.100416

Adane, T., Haile, D., Dessie, A., Abebe, Y., & Dagne, H. (2020). Response surface methodology as a statistical tool for optimization of removal of chromium (VI) from aqueous solution by Teff (Eragrostis teff) husk activated carbon. Applied Water Science, 10(1), 1–13. https://doi.org/10.1007/s13201-019-1120-8

Ahmad, F. A. (2023). The use of agro-waste-based adsorbents as sustainable, renewable, and low-cost alternatives for the removal of ibuprofen and carbamazepine from water. In Heliyon (Vol. 9, Issue 6). Elsevier Ltd. https://doi.org/10.1016/j.heliyon.2023.e16449

AlNeyadi, S. S., SA, S., Aljasmi, S. N., Alshkeili, D. S., Al Anoud, M. H., & Salama, O. S. (2024). Ibuprofen removal from water using the IB-COF covalent organic framework. Journal of Hazardous Materials Advances, 15. https://doi.org/10.1016/j.hazadv.2024.100451

Al-Obaidi, N. S., Sadeq, Z. E., Mahmoud, Z. H., Abd, A. N., Al-Mahdawi, A. S., & Ali, F. K. (2023). Synthesis of Chitosan-TiO2 Nanocomposite for Efficient Cr(VI) Removal from Contaminated Wastewater Sorption Kinetics, Thermodynamics and Mechanism. Journal of Oleo Science, 72(3), 337–346. https://doi.org/10.5650/jos.ess22335

Alqarni, L. S., Algethami, J. S., EL Kaim Billah, R., Alorabi, A. Q., Alnaam, Y. A., Algethami, F. K., Bahsis, L., Jawad, A. H., Wasilewska, M., & López-Maldonado, E. A. (2024). A novel chitosan-alginate@Fe/Mn mixed oxide nanocomposite for highly efficient removal of Cr (VI) from wastewater: Experiment and adsorption mechanism. International Journal of Biological Macromolecules, 263(February). https://doi.org/10.1016/j.ijbiomac.2024.129989

Aranaz, I., Alcántara, A. R., Civera, M. C., Arias, C., Elorza, B., Caballero, A. H., & Acosta, N. (2021). Chitosan: An overview of its properties and applications. In Polymers (Vol. 13, Issue 19). MDPI. https://doi.org/10.3390/polym13193256

Banerjee, S., & Maric, F. (2023). Mitigating the environmental impact of NSAIDs - physiotherapy as a contribution to One Health and the SDGs. European Journal of Physiotherapy, 25(1), 51–55. https://doi.org/10.1080/21679169.2021.1976272

Chopra, S., & Kumar, D. (2020). Ibuprofen as an emerging organic contaminant in environment, distribution and remediation. In Heliyon (Vol. 6, Issue 6). Elsevier Ltd. https://doi.org/10.1016/j.heliyon.2020.e04087

da Silva, K. A., de Carvalho Arabidian, V., Gonçalves, J. O., Vieira, M. L. G., Barbosa, S. C., Primel, E. G., de Almeida Pinto, L. A., & Junior, T. R. S. C. (2024). Application of effective cross-linked chitosan-based aerogel adsorbent for removal of ibuprofen from water. Polymer Bulletin. https://doi.org/10.1007/s00289-024-05551-z

Davarnejad, R., Soofi, B., Farghadani, F., & Behfar, R. (2018). Ibuprofen removal from a medicinal effluent: A review on the various techniques for medicinal effluents treatment. In Environmental Technology and Innovation (Vol. 11, pp. 308–320). Elsevier B.V. https://doi.org/10.1016/j.eti.2018.06.011

Dehghanpour, H. R. (2020). pH, molar ratio of ferrous to ferric ions and surfactant presence effects on physical properties of iron oxide nanoparticles generated by co-precipitation method. Journal of Coordination Chemistry, 73(24), 3452–3464. https://doi.org/10.1080/00958972.2020.1849639

de Souza, L. Z. M., Pinto, B. C., Alves, A. B., de Oliveira Ribeiro, A. V., Teodoro Feliciano, D. C., da Silva, L. H., Moraes Dias, T. T., Yılmaz, M., de Oliveira, M. A., da Silva Bezerra, A. C., Ferreira, O. E., de Lima, R. P., do Santos Pimenta, L. P., & Teixeira Machado, A. R. (2022). Ecotoxicological Effects of Biochar Obtained from Spent Coffee Grounds. Materials Research, 25. https://doi.org/10.1590/1980-5373-MR-2022-0013

Dima, A. A., Zewge, F., & Chebude, Y. (2023). Adsorption activity of spent coffee ground biochar for the removal of Vivizole Red 3BS dye from aqueous solution. https://doi.org/10.21203/rs.3.rs-2582956/v1

Eapen, J. V., Thomas, S., Antony, S., George, P., & Antony, J. (2024). A review of the effects of pharmaceutical pollutants on humans and aquatic ecosystem. Exploration of Drug Science, 484–507. https://doi.org/10.37349/eds.2024.00058

Egbedina, A. O., Odejobi, S. B., Akinbile, B. J., Ambushe, A. A., Olu-Owolabi, B. I., & Adebowale, K. O. (2023). A porous bentonite-coconut husk composite for the enhanced adsorption of selected emerging contaminants from aqueous solution. Environmental Science: Advances, 2(11), 1554–1565. https://doi.org/10.1039/d3va00033h

Eivazzadeh-Keihan, R., Pajoum, Z., Aliabadi, H. A. M., Mohammadi, A., Kashtiaray, A., Bani, M. S., Pishva, B., Maleki, A., Heravi, M. M., Mahdavi, M., & Ziaei Ziabari, E. (2023). Magnetized chitosan hydrogel and silk fibroin, reinforced with PVA: a novel nanobiocomposite for biomedical and hyperthermia applications. RSC Advances, 13(13), 8540–8550. https://doi.org/10.1039/d3ra00612c

Gkika, D. A., Mitropoulos, A. C., Kokkinos, P., Lambropoulou, D. A., Kalavrouziotis, I. K., Bikiaris, D. N., & Kyzas, G. Z. (2023). Modified chitosan adsorbents in pharmaceutical simulated wastewaters: A review of the last updates. Carbohydrate Polymer Technologies and Applications, 5. https://doi.org/10.1016/j.carpta.2023.100313

Gutierrez, F. V., Lima, I. S., De Falco, A., Ereias, B. M., Baffa, O., Diego de Abreu Lima, C., Morais Sinimbu, L. I., de la Presa, P., Luz-Lima, C., & Damasceno Felix Araujo, J. F. (2024). The effect of temperature on the synthesis of magnetite nanoparticles by the coprecipitation method. Heliyon, 10(4). https://doi.org/10.1016/j.heliyon.2024.e25781

Inayat, A., Rocha-Meneses, L., Said, Z., Ghenai, C., Ahmad, F. F., Al-Ali, A. M., Mahmood, F., & Abdallah, N. (2022). Activated Carbon Production from Coffee Waste via Slow Pyrolysis Using a Fixed Bed Reactor. Environmental and Climate Technologies, 26(1), 720–729. https://doi.org/10.2478/rtuect-2022-0055

Jan-Roblero, J., & Cruz-Maya, J. A. (2023). Ibuprofen: Toxicology and Biodegradation of an Emerging Contaminant. In Molecules (Vol. 28, Issue 5). MDPI. https://doi.org/10.3390/molecules28052097

Jeníček, L., Tunklová, B., Malaťák, J., Neškudla, M., & Velebil, J. (2022). Use of Spent Coffee Ground as an Alternative Fuel and Possible Soil Amendment. Materials, 15(19). https://doi.org/10.3390/ma15196722

Karaer Yağmur, H. (2020). Preparation and Characterization of Polyvinyl Alcohol/Activated Carbon (PVA/AC) Composite and Its Use in the Adsorption of 4-Nitrophenol (4-NP). Adiyaman University Journal of Science, 10(1), 160–178. https://doi.org/10.37094/adyujsci.628399

Kassahun, S. K., Getaye, A., Tsigkou, K., & Angelidaki, I. (2025). Coffee processing waste as a reinforcing material in the preparation of chitosan-based magnetic composite for the removal of chromium (VI) from aqueous solution. Results in Engineering, 26. https://doi.org/10.1016/j.rineng.2025.105455

Kassahun, S. K., Kiflie, Z., Kim, H., & Baye, A. F. (2021). Process optimization and kinetics analysis for photocatalytic degradation of emerging contaminant using N-doped TiO2-SiO2 nanoparticle: Artificial Neural Network and Surface Response Methodology approach. Environmental Technology and Innovation, 23. https://doi.org/10.1016/j.eti.2021.101761

Kaur, H., Singh, S., Rode, S., Chaudhary, P. K., Khan, N. A., Ramamurthy, P. C., Gupta, D. N., Kumar, R., Das, J., & Sharma, A. K. (2024). Fabrication and characterization of polyvinyl alcohol-chitosan composite nanofibers for carboxylesterase immobilization to enhance the stability of the enzyme. Scientific Reports, 14(1). https://doi.org/10.1038/s41598-024-67913-x

Khierallah, A. H. I., Bates, I. I. C., Chabot, B., & Lajeunesse, A. (2021). Adsorption of Pharmaceutical Contaminants from Aqueous Solutions Using N,O-Carboxymethyl Chitosan/Polyethylene Oxide (PEO) Electrospun Nanofibers. Journal of Materials Science and Chemical Engineering, 09(11), 15–38. https://doi.org/10.4236/msce.2021.911003

Kumar, R., & Barakat, M. A. (2024). Flexible multifunctional chitosan/graphene oxide/polyaniline hydrogel thin films for adsorption of ibuprofen from aqueous solution. Cellulose, 31(7), 4347–4366. https://doi.org/10.1007/s10570-024-05891-z

Lekene, R. B. N., Ntep, T. M. M., Fetzer, M. N. A., Strothmann, T., Nsami, J. N., & Janiak, C. (2023). The efficient removal of ibuprofen, caffeine, and bisphenol A using engineered egusi seed shells biochar: adsorption kinetics, equilibrium, thermodynamics, and mechanism. Environmental Science and Pollution Research, 30(44), 100095–100113. https://doi.org/10.1007/s11356-023-29377-w

Lessa, E. F., Nunes, M. L., & Fajardo, A. R. (2018). Chitosan/waste coffee-grounds composite: An efficient and eco-friendly adsorbent for removal of pharmaceutical contaminants from water. Carbohydrate Polymers, 189, 257–266. https://doi.org/10.1016/j.carbpol.2018.02.018

Le, V. T., Pham, T. M., Doan, V. D., Lebedeva, O. E., & Nguyen, H. T. (2019). Removal of Pb(ii) ions from aqueous solution using a novel composite adsorbent of Fe3o4/PVA/spent coffee grounds. Separation Science and Technology (Philadelphia), 54(18), 3070–3081. https://doi.org/10.1080/01496395.2019.1565770

Liakos, E. V., Lazaridou, M., Michailidou, G., Koumentakou, I., Lambropoulou, D. A., Bikiaris, D. N., & Kyzas, G. Z. (2021). Chitosan Adsorbent Derivatives for Pharmaceuticals Removal from Effluents: A Review. In Macromol (Vol. 1, Issue 2, pp. 130–154). Multidisciplinary Digital Publishing Institute (MDPI). https://doi.org/10.3390/macromol1020011

Lin, L., Yang, H., & Xu, X. (2022). Effects of Water Pollution on Human Health and Disease Heterogeneity: A Review. In Frontiers in Environmental Science (Vol. 10). Frontiers Media S.A. https://doi.org/10.3389/fenvs.2022.880246

Mahmood Aljamali, N., & Obaid Alfatlawi, I. (2021). Physical and Chemical Adsorption and its Applications. https://doi.org/10.37628/IJTCK

Mali, A., Bhilare, S., Chaudhari, B., & Redasani, V. (2024). Development and Validation of UV Spectrophotometric Method for the Determination of Ibuprofen by Using Quality by Design (QbD) Approach. International Journal of Pharmaceutical Sciences Review and Research, 84(6). https://doi.org/10.47583/ijpsrr.2024.v84i06.014

Mardana, P., & Arjana, I. G. (2024). Synthesis of Magnetite Nanoparticles (Fe3O4) Based on Taman River Sand Magnetic Material. Indonesian Physical Review, 7(3), 327–337. https://doi.org/10.29303/ipr.v

Mojiri, A., Kazeroon, R. A., & Gholami, A. (2019). Cross-linked magnetic chitosan/activated biochar for removal of emerging micropollutants from water: Optimization by the artificial neural network. Water (Switzerland), 11(3). https://doi.org/10.3390/w11030551

Munzhelele, E. P., Mudzielwana, R., Ayinde, W. B., & Gitari, W. M. (2024). Pharmaceutical Contaminants in Wastewater and Receiving Water Bodies of South Africa: A Review of Sources, Pathways, Occurrence, Effects, and Geographical Distribution. In Water (Switzerland) (Vol. 16, Issue 6). Multidisciplinary Digital Publishing Institute (MDPI). https://doi.org/10.3390/w16060796

Murtaza, G., Ahmed, Z., Dai, D. Q., Iqbal, R., Bawazeer, S., Usman, M., Rizwan, M., Iqbal, J., Akram, M. I., Althubiani, A. S., Tariq, A., & Ali, I. (2022). A review of mechanism and adsorption capacities of biochar-based engineered composites for removing aquatic pollutants from contaminated water. In Frontiers in Environmental Science (Vol. 10). Frontiers Media S.A. https://doi.org/10.3389/fenvs.2022.1035865

Nagarajan, T., Binti Mohd Fekeri, N. H., Raju, G., Shanmugan, S., Jeppu, G., Walvekar, R., Rustagi, S., & Khalid, M. (2024). Adsorption parameters optimization of spent coffee ground biochar for methylene blue removal using response surface methodology. Chemosphere, 364. https://doi.org/10.1016/j.chemosphere.2024.143242

Ngernyen, Y., Petsri, D., Sribanthao, K., Kongpennit, K., Pinijnam, P., Pedsakul, R., & Hunt, A. J. (2023). Adsorption of the non-steroidal anti-inflammatory drug (ibuprofen) onto biochar and magnetic biochar prepared from chrysanthemum waste of the beverage industry. RSC Advances, 13(21), 14712–14728. https://doi.org/10.1039/d3ra01949g

Oliveira, G. A., Gevaerd, A., Mangrich, A. S., Marcolino-Junior, L. H., & Bergamini, M. F. (2021). Biochar obtained from spent coffee grounds: Evaluation of adsorption properties and its application in a voltammetric sensor for lead (II) ions. Microchemical Journal, 165. https://doi.org/10.1016/j.microc.2021.106114

Omidvar-motlagh, M., Es, Z., & Hosseini, H. A. (2023). Eco-Friendly Adsorptive Removal of Chromium From Water and Wastewater by Nano Sodium Bentonite. 10(2), 44–60. https://doi.org/10.30473/ijac.2023.69100.1274

Ortúzar, M., Esterhuizen, M., Olicón-Hernández, D. R., González-López, J., & Aranda, E. (2022). Pharmaceutical Pollution in Aquatic Environments: A Concise Review of Environmental Impacts and Bioremediation Systems. In Frontiers in Microbiology (Vol. 13). Frontiers Media S.A. https://doi.org/10.3389/fmicb.2022.869332

Osman, A. I., Ayati, A., Farghali, M., Krivoshapkin, P., Tanhaei, B., Karimi-Maleh, H., Krivoshapkina, E., Taheri, P., Tracey, C., Al-Fatesh, A., Ihara, I., Rooney, D. W., & Sillanpaä, M. (2024). Advanced adsorbents for ibuprofen removal from aquatic environments: a review. In Environmental Chemistry Letters (Vol. 22, Issue 1, pp. 373–418). Springer Science and Business Media Deutschland GmbH. https://doi.org/10.1007/s10311-023-01647-6

Placova, K., Halfar, J., Brozova, K., & Heviankova, S. (2023). Issues of Non-Steroidal Anti-Inflammatory Drugs in Aquatic Environments: A Review Study †. Engineering Proceedings, 57(1). https://doi.org/10.3390/engproc2023057013

Pot E, J., Milakovic, M., Chaumot, A., Seidensticker, S., Melling, M., Supriatin, A., & Sherif, S. (2022). Pharmaceutical pollution of the world's rivers. https://doi.org/10.1073/pnas.2113947119/-/DCSupplemental

Rashid Ahmed, H., Kayani, K. F., Mary Ealias, A., & George, G. (2024). Biochar as an eco-friendly adsorbent for ibuprofen removal via adsorption: A review. In Inorganic Chemistry Communications (Vol. 170). Elsevier B.V. https://doi.org/10.1016/j.inoche.2024.113397

Samal, K., Mahapatra, S., & Hibzur Ali, M. (2022). Pharmaceutical wastewater as Emerging Contaminants (EC): Treatment technologies, impact on environment and human health. In Energy Nexus (Vol. 6). Elsevier Ltd. https://doi.org/10.1016/j.nexus.2022.100076

Saxena, R., Laddha, H., & Bhoi, R. G. (2024). Sustainable management of spent coffee grounds: applications, decompositions techniques and structural analysis. In Journal of Material Cycles and Waste Management. Springer. https://doi.org/10.1007/s10163-024-02113-3

S, D. L., B, V. G., & Murali, V. (2024). From prescription to pollution: The ecological consequences of NSAIDs in aquatic ecosystems. In Toxicology Reports (Vol. 13). Elsevier Inc. https://doi.org/10.1016/j.toxrep.2024.101775

Shaheen, J. F., Eniola, J. O., & Sizirici, B. (2024). Adsorption of ibuprofen from aqueous solution by modified date palm biochar: Performance, optimization, and life cycle assessment. Bioresource Technology Reports, 25. https://doi.org/10.1016/j.biteb.2023.101696

Shaheen, S. M., Mosa, A., Natasha, Abdelrahman, H., Niazi, N. K., Antoniadis, V., Shahid, M., Song, H., Kwon, E. E., & Rinklebe, J. (2022). Removal of toxic elements from aqueous environments using nano zero-valent iron- and iron oxide-modified biochar: a review. In Biochar (Vol. 4, Issue 1). Springer. https://doi.org/10.1007/s42773-022-00149-y

Shin, J., Kwak, J., Lee, Y. G., Kim, S., Choi, M., Bae, S., Lee, S. H., Park, Y., & Chon, K. (2021). Competitive adsorption of pharmaceuticals in lake water and wastewater effluent by pristine and NaOH-activated biochars from spent coffee wastes: Contribution of

hydrophobic and π-π interactions. Environmental Pollution, 270. https://doi.org/10.1016/j.envpol.2020.116244

Singh, T. A., Pal, N., Sharma, P., & Passari, A. K. (2023). Spent coffee ground: transformation from environmental burden into valuable bioactive metabolites. In Reviews in Environmental Science and Biotechnology (Vol. 22, Issue 4, pp. 887–898). Springer Science and Business Media B.V. https://doi.org/10.1007/s11157-023-09669-w

Song, Q., Gao, J., Lin, Y., Zhang, Z., & Xiang, Y. (2020). Synthesis of cross-linking chitosan-PVA composite hydrogel and adsorption of Cu(II) ions. Water Science and Technology, 81(5), 1063–1070. https://doi.org/10.2166/wst.2020.204

Sopanrao, K. S., & Sreedhar, I. (2024). Polyvinyl alcohol modified chitosan composite as a novel and efficient adsorbent for multi-metal removal. Separation and Purification Technology, 340. https://doi.org/10.1016/j.seppur.2024.126731

Sunyoto, N. M. S., Setyawan, H. Y., Dewi, I. A., Widyasari, Y. E., Putri, M. R., & Santoso, R. A. M. (2022). Coffee Spent Ground-Based Biochar's Properties and Application: A Systematic Review. IOP Conference Series: Earth and Environmental Science, 1018(1). https://doi.org/10.1088/1755-1315/1018/1/012036

Tegegne, A. A., Mekasha, Y. T., Ayu, A. A., Hasen, G., & Suleman, S. (2024). A review on emerging pharmaceutical residues in Ethiopia: occurrence, ecotoxicological aspects, and regulatory concerns. In Frontiers in Microbiology (Vol. 15). Frontiers Media SA. https://doi.org/10.3389/fmicb.2024.1499487

Trianda, Y., Adityosulindro, S., & Moersidik, S. S. (2024). Ibuprofen as an Emerging Contaminant of Concern: Occurrence in Southeast Asia Water Environment. E3S Web of Conferences, 530. https://doi.org/10.1051/e3sconf/202453002007

Tsigkou, K., Demissie, B. A., Hashim, S., Ghofrani-Isfahani, P., Thomas, R., Mapinga, K. F., Kassahun, S. K., & Angelidaki, I. (2025). Coffee processing waste: Unlocking opportunities for sustainable development. In Renewable and Sustainable Energy Reviews (Vol. 210). Elsevier Ltd. https://doi.org/10.1016/j.rser.2024.115263

Umejuru, E. C., Prabakaran, E., & Pillay, K. (2023). Coal Fly Ash Decorated with Graphene and Polyaniline Nanocomposites for Effective Adsorption of Hexavalent Chromium and

Its Reuse for Photocatalysis. ACS Omega, 8(20), 17523–17537. https://doi.org/10.1021/acsomega.2c05352

Vasilachi, I. C., Asiminicesei, D. M., Fertu, D. I., & Gavrilescu, M. (2021). Occurrence and fate of emerging pollutants in water environment and options for their removal. In Water (Switzerland) (Vol. 13, Issue 2). MDPI AG. https://doi.org/10.3390/w13020181

Verhoeven, J. E., Han, L. K. M., Lever-van Milligen, B. A., Hu, M. X., Révész, D., Hoogendoorn, A. W., Batelaan, N. M., van Schaik, D. J. F., van Balkom, A. J. L. M., van Oppen, P., & Penninx, B. W. J. H. (2023). Antidepressants or running therapy: Comparing effects on mental and physical health in patients with depression and anxiety disorders. Journal of Affective Disorders, 329, 19–29. https://doi.org/10.1016/j.jad.2023.02.064

Wang, J., & Guo, X. (2020). Adsorption kinetic models: Physical meanings, applications, and solving methods. In Journal of Hazardous Materials (Vol. 390). Elsevier B.V. https://doi.org/10.1016/j.jhazmat.2020.122156

Xing, T., Wu, Y., Wang, Q., Sadrnia, A., Behmaneshfar, A., & Dragoi, E. N. (2023). Adsorption of ibuprofen using waste coffee derived carbon architecture: Experimental, kinetic modeling, statistical and bio-inspired optimization. Environmental Research, 231. https://doi.org/10.1016/j.envres.2023.116223

Yang, Y., Wan, Y., Chen, J., Chen, H., Li, Y., Muñoz-Carpena, R., Zheng, Y., Huang, J., Zhang, Y., & Gao, B. (2025). Ball-Milled Spent Coffee Ground Biochar Effectively Removes Caffeine from Water. Water (Switzerland), 17(6). https://doi.org/10.3390/w17060881

Yeliz Ozudogru, & Ecem Tekne. (2023). Adsorption of Methylene Blue from Aqueous Solution Using Spent Coffee/Chitosan Composite. Journal of Water Chemistry and Technology, 45(3), 234–245. https://doi.org/10.3103/s1063455x23030086

Yusmaniar, Y., Julio, E., Rahman, A., Yudanto, S. D., & Susetyo, F. B. (2023). Synthesis of Polyvinyl Alcohol-Chitosan Composite Film using Nanocellulose from Coconut Fibers (Cocos nucifera). International Journal of Engineering, Transactions A: Basics, 36(11), 1993–2003. https://doi.org/10.5829/ije.2023.36.11b.05

Zhang, J., Zhang, X., Li, X., Li, W., Mao, S., He, S., Wu, X., Tang, C., Yu, J., Pan, L., & Zhou, X. (2024). High efficiency removal of ibuprofen in water using activated carbon derived

from Radix Angelica Dahurica residue. Environmental Progress and Sustainable Energy, 43(3). https://doi.org/10.1002/ep.14318

Zuluaga, R., Hoyos, C. G., Velásquez-Cock, J., Vélez-Acosta, L., Palacio Valencia, I., Rodríguez Torres, J. A., & Gañán Rojo, P. (2024). Exploring Spent Coffee Grounds: Comprehensive Morphological Analysis and Chemical Characterization for Potential Uses. Molecules, 29(24). https://doi.org/10.3390/molecules29245866

Zungu, V., Hadebe, L., Mpungose, P., Hamza, I., Amaku, J., & Gumbi, B. (2022). Fabrication of Biochar Materials from Biowaste Coffee Grounds and Assessment of Its Adsorbent Efficiency for Remediation of Water-Soluble Pharmaceuticals. Sustainability (Switzerland), 14(5). https://doi.org/10.3390/su14052931

APPENDICES

Appendix A: Design Expert Model Summary

Table A.1: Build information for the model

File Version	13.0.5.0		
Study Type	RSM	Sub Type	Randomized
Design Type	CCD	Runs	30
Design Model	Quadratic	Blocks	No Blocks

Table A.2: Model summary statistics

Source	**Std. Dev.**	**R^2**	**Adjusted R^2**	**Predicted R^2**	**PRESS**	
Linear	8.51	0.7569	0.7180	0.6257	2785.31	
2FI	9.52	0.7684	0.6466	0.6247	2792.60	
Quadratic	**1.65**	**0.9945**	**0.9894**	**0.9713**	**213.56**	**Suggested**
Cubic	0.9507	0.9991	0.9965	0.9754	182.77	Aliased

Appendix B: Design Expert Model Equations

Table B.1: Coefficients in terms of coded factors

Factors	Coefficient Estimate	Df	Standard Error	95% CI Low	95% CI High	VIF
Intercept	75.53	1	0.6742	74.09	76.96	
A-pH	-7.32	1	0.3371	-8.04	-6.60	1.0000
B-Concentration of IBP	-4.72	1	0.3371	-5.44	-4.00	1.0000
C-Dosage	6.81	1	0.3371	6.09	7.52	1.0000
D-Time	10.61	1	0.3371	9.89	11.33	1.0000
AB	-1.76	1	0.4129	-2.64	-0.8767	1.0000
AC	0.6763	1	0.4129	-0.2037	1.56	1.0000
AD	-0.0774	1	0.4129	-0.9574	0.8025	1.0000
BC	1.22	1	0.4129	0.3438	2.10	1.0000
BD	0.3525	1	0.4129	-0.5275	1.23	1.0000
CD	0.4452	1	0.4129	-0.4348	1.33	1.0000
A^2	-6.86	1	0.3153	-7.53	-6.18	1.05
B^2	2.36	1	0.3153	1.68	3.03	1.05
C^2	0.9994	1	0.3153	0.3273	1.67	1.05
D^2	-1.02	1	0.3153	-1.69	-0.3449	1.05

Table B.2: Actual and coded model equations

Actual Equation		**Coded Equation**	
IBP Removal efficiency	=	IBP Removal efficiency	=
+26.51286		+75.53	
+18.64777	pH	-7.32	A
-7.32724	Conc	-4.72	B
-12.45251	Dosage	+6.81	C
+0.727439	Time	+10.61	D
-0.351343	pH * conc	-1.76	AB
+0.676259	pH * dosage	+0.6763	AC
-0.001936	pH * time	-0.0774	AD
+0.979035	conc * dosage	+1.22	BC
+0.007050	conc * time	+0.3525	BD
+0.044522	dosage * time	+0.4452	CD
-1.71423	pH^2	-6.86	A^2
+0.377114	$conc^2$	+2.36	B^2
+3.99760	$dosage^2$	+0.9994	C^2
-0.002543	$time^2$	-1.02	D^2

Appendix C: Laboratory Procedures (Photographs)

Figure C.1: Photograph confirmations for Experimental procedures